ELSEVIER

Advances in Colloid and Interface Science 136 (2008) 45–64

ADVANCES IN COLLOID AND INTERFACE SCIENCE

www.elsevier.com/locate/cis

Template-based synthesis of nanorod, nanowire, and nanotube arrays

Guozhong Cao *, Dawei Liu

Department of Materials Science and Engineering, University of Washington, Seattle, WA 98195

Available online 26 July 2007

Abstract

This review introduces and summarizes the fundamentals and various technical approaches developed for the template-based synthesis of nanorod, nanowire and nanotube arrays. After a brief introduction to various concepts for the growth of nanorods, nanowires and nanobelts, attention will be focused mainly on the most widely used and well established techniques for the template-based growth of nanorod arrays: electrochemical deposition, electrophoretic deposition, filling of templates by capillary force and centrifugation, and chemical conversion. In each section, relevant fundamentals will be first introduced, followed with examples to illustrate the specific details of each technique.

Keywords: Nanorod arrays; Template-based synthesis; Solution; Colloidal based synthesis

Contents

* Corresponding author. Tel.: +1 206 616 9084; fax: +1 206 543 3100.
E-mail address: gzcao@u.washington.edu (G. Cao).

0001-8686/$ - see front matter © 2007 Elsevier B.V. All rights reserved.
doi:10.1016/j.cis.2007.07.003

1. Introduction

Synthesis, characterization and application of nanowires, nanorods, nanotubes, and nanobelts (also often referred to as one-dimensional nanostructure) comprise a significant aspect of today's endeavor in nanotechnology. Many techniques have been developed along with a significantly enhanced fundamental understanding [1–5], though the field is involving rapidly with new synthesis methods and new nanowires or nanorods reported in literature. For the growth of nanowires and nanorods, evaporation–condensation growth has been successfully demonstrated for the synthesis of various oxide nanowires and nanorods. Similarly, dissolution–condensation method has been widely used for the synthesis of various metallic nanowires from solutions. Vapor–liquid–solid (VLS) growth method is a very versatile approach; various elementary and compound semiconductor nanowires have been synthesized by this method [6]. Template-based growth of nanowires or nanorods is an even more versatile method for various materials. Substrate ledge or step induced growth of nanowires or nanorods has also been under intensive investigation [7]. Except the VLS and template-based growth, most of the above mentioned methods result in randomly oriented nanowires or nanorods (commonly in the form of powder). As explicitly indicated in its name, VLS is a vapor deposition method with the assistance of catalyst [8,9]. VLS method offers the possibility to grow well oriented nanorods or nanowires directly attached to the substrates, and thus is often advantageous for subsequent characterization and applications; however, special catalysts are required to form a liquid capsule at the advancing surface during growth at elevated temperatures. In addition, the possible incorporation of catalyst into nanowires and the difficulty to remove such capsules from the tip of nanowires or nanorods are two setbacks. Template-based growth is commonly a solution or colloidal dispersion based process. It is less expensive and readily scalable to mass production. The diameter, density and length of nanorods and nanowires are easily controlled independently. It also offers the advantages of less contamination and is environmentally benign. However, template-based synthesis suffers from the polycrystalline nature of the resultant nanowires and nanorods, in addition to the difficulties to find appropriate templates with pore channels of desired diameter, length and surface chemistry and to remove the template completely without compromising the integrity of grown nanowires or nanorods. This review will focus mainly on the template-based synthesis of nanorod and nanowire arrays; however, template assisted synthesis of nanotube arrays is also discussed. It should also be noted that the terms of nanorod and nanowire are used interchangeably without special distinction in this review, as commonly seen in open literature.

In comparison with nanostructured materials in other forms, nanorod arrays offer several advantages for property study and practical applications. A significant progress has been made in the study on the physical properties of individual nanowires and nanorods by direct measuring the properties of individual nanostructures. However, such studies generally require dedicated preparation of experimental set-up and execution of measurements. For example, for the electrical conductivity measurement, patterned electrodes on a substrate are first created and, then, nanowires or nanorods are dispersed in an appropriate solvent or solution. Such prepared nanowire colloidal dispersion casts on the substrate with pattern electrodes. Measurements would be carried out after identifying individual nanowires or nanorods bridging two electrodes. There is very limited option for manipulation of nanowires or nanorods, and it is difficult to improve the contact between the sample and the electrodes to ensure a desired ohmic contact. For practical applications, the output or signals generated by single nanowire or nanorod based devices is small, signal to noise ratio is small, and thus highly sensitive instrumentation is required to accommodate such devices.

2. Template-based approach

The template approach has been extensively investigated in the synthesis of various nanostructures. For example, mesoporous oxides with well defined and ordered porous structure can be readily synthesized using surfactant or copolymer micelles as templates through sol–gel processing [10,11]. Another recent example is Au nanoparticle templated synthesis of poly(*N*-isopropoylacrylamide) nanogels [12]. However, template-based synthesis is most commonly and widely used to prepare free-standing, non-oriented and oriented nanowires or nanorods or nanotubes; the latter is also referred to as nanorod or nanowire or nanotube arrays. The most commonly used and commercially available templates are anodized alumina membrane (AAM) [13] and radiation track-etched polycarbonate (PC) membranes [14].Other membranes have also been used, such as nanochannel array on glass [15], radiation track-etched mica [16], mesoporous materials [17], porous silicon by electrochemical etching of silicon wafer [18], zeolites [19] and carbon nanotubes [20,21]. Bio-templates are also explored for the growth of nanowires [22] and nanotubes [23], such as Cu [24], Ni [22], Co [22], and Au [25] nanowires. The commonly used alumina membranes with uniform and parallel pores are made by anodic oxidation of aluminum sheet in solutions of sulfuric, oxalic, or phosphoric acids [13,26]. The pores can be arranged in a regular hexagonal array, and densities as high as 10^{11} pores/cm^2 can be achieved [27]. Pore size ranging from 10 nm to 100 μm can be made [27,28]. PC membranes are made by bombarding a nonporous polycarbonate sheet, typically 6 to 20 μm in thickness, with nuclear fission fragments to create damage tracks, and then chemically etching these tracks into pores [14]. In these radiation track etched membranes, pores have a uniform size as small as 10 nm, but they are randomly distributed. Pore densities can be as high as 10^9 pores/cm^2.

In addition to the desired pore or channel size, morphology, size distribution and density of pores, template materials must meet certain requirements. First, the template materials must be compatible with the processing conditions. For example, an electrical insulator is required for a template to be used in electrochemical deposition. Except for the template-directed synthesis, template materials should be chemically and thermally inert during the synthesis and following processing

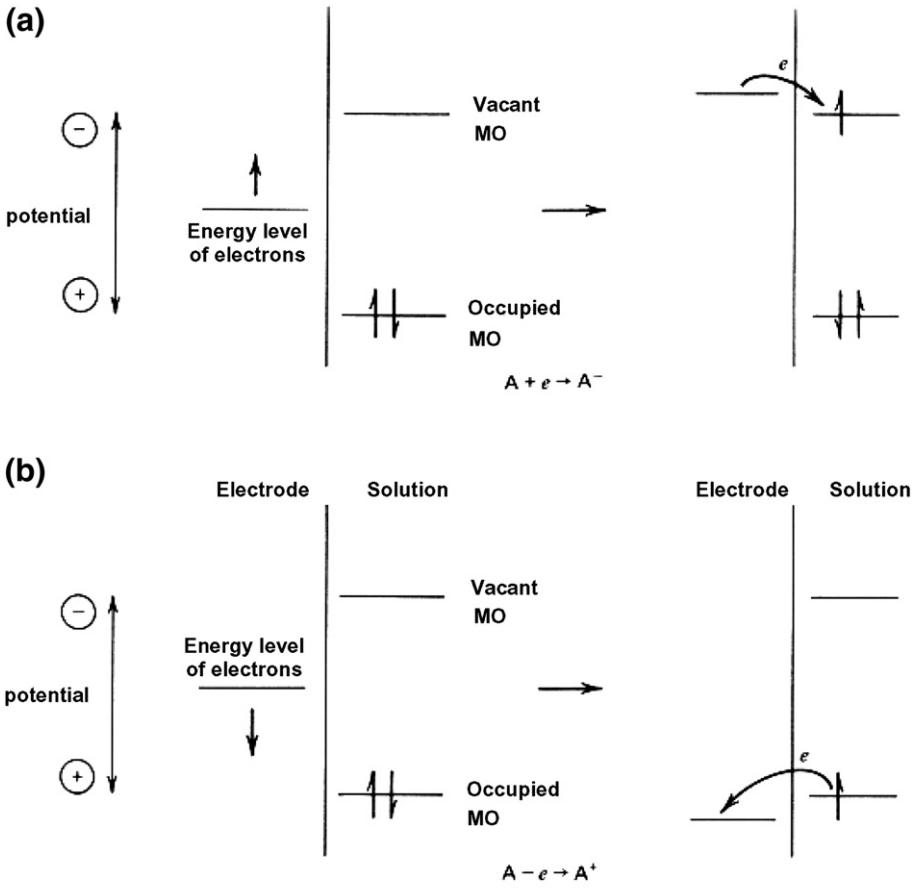

Fig. 1. Representation of (a) reduction and (b) oxidation process of a species A in solution. The molecular orbitals (MO) of species A shown are the highest occupied MO and the lowest vacant MO. As shown, these correspond in an approximate way to the E_0's of the A/A^- and A^+/A couples, respectively. [A.J. Bard and L.R. Faulkner, Electrochemical Methods, John Wiley & Sons, New York, 1980].

steps. Secondly, depositing materials or solution must wet the internal pore walls. Thirdly, for the synthesis of nanorods or nanowires, the deposition should start from the bottom or one end of the template channels and proceed from one side to another. However, for the growth of nanotubules, the deposition should start from the pore wall and proceed inwardly. Inward

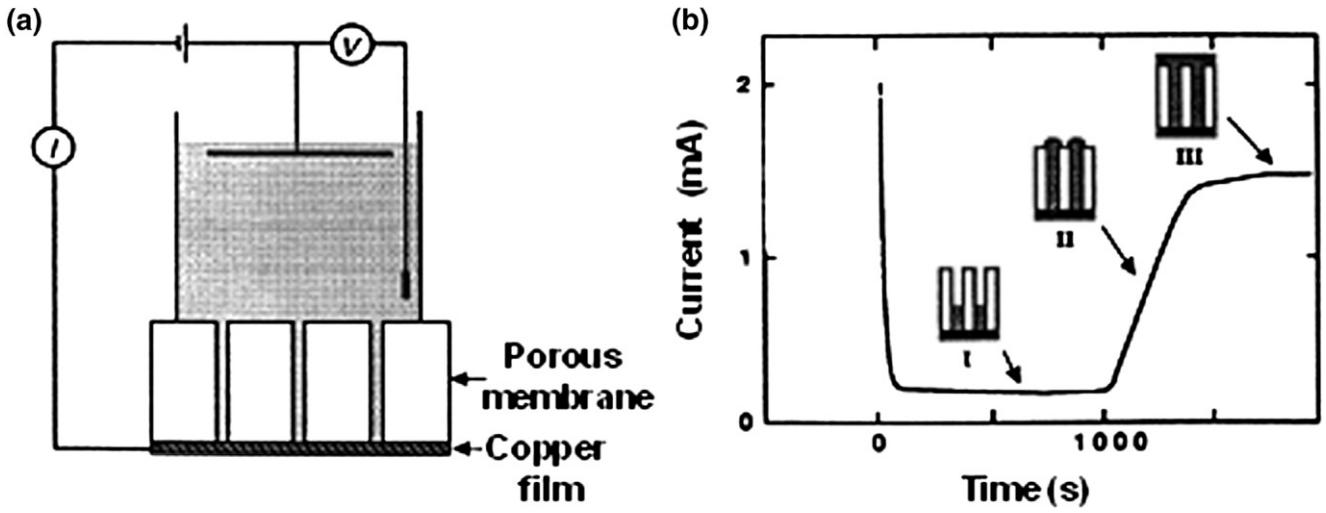

Fig. 2. Common experimental set-up for the template-based growth of nanowires using electrochemical deposition. (a) Schematic illustration of electrode arrangement for deposition of nanowires. (b) Current–time curve for electrodeposition of Ni into a polycarbonate membrane with 60 nm diameter pores at −1.0 V. Insets depict the different stages of the electrodeposition. [T.M. Whitney, J.S. Jiang, P.C. Searson, and C.L. Chien, Science 261 (1993) 1316].

growth may result in the pore blockage, so that should be avoided in the growth of "solid" nanorods or nanowires. Kinetically, enough surface relaxation permits maximal packing density, so a diffusion-limited process is preferred. Other considerations include the easiness of release of nanowires or nanorods from the templates and of handling during the experiments.

AAM and PC membranes are most commonly used for the synthesis of nanorod or nanowire arrays. Both templates are very convenient to use during the growth of nanorods by various growth mechanisms, but each type of template also offers a few disadvantages. The advantage of using PC as the template is its easy handling and easy removal by means of pyrolysis at elevated temperatures, but the flexibility of PC is more prone to distortion during the heating process, and the removal of the template would occur before complete densification of the nanorods. These factors would result in broken and deformed nanorods. The advantage of using AAM as the template is its rigidity and resistance to high temperatures, allowing for the nanorods to densify completely before removal. This would result in a larger surface area of fairly free-standing and unidirectionally-aligned nanorod arrays. The problem with AAM is the complete removal of the template after nanorod growth, which has so far been unsuccessful using wet-chemical etching.

3. Electrochemical deposition

Electrochemical deposition, also known as electrodeposition, involves oriented diffusion of charged reactive species through a solution when an external electric field is applied, and reduction of the charged growth species at the growth or deposition surface which also serves as an electrode. In industry, electrochemical deposition is widely used in making metallic coatings in a process known as electroplating [29]. In general, this method is only applicable to electrical conductive materials such as metals, alloys, semiconductors, and electrically conductive polymers and oxides. After the initial deposition, the electrode is separated from the depositing solution by the deposit and the electrical current must go through the deposit to allow the deposition process to continue. When deposition is confined inside the pores of template membranes, nanocomposites are produced. If the template membrane is removed, nanorod or nanowire arrays are prepared. However, when the deposition occurs along the wall surface of the pore channels, nanotubes would form.

When a solid immerses in a polar solvent or an electrolyte solution, surface charge will develop. The electrode potential is described by the Nernst equation:

$$E = E_0 + \frac{RT}{n_i F}\ln(a_i) \quad (1)$$

where E_0 is the standard electrode potential, or the potential difference between the electrode and the solution, when the activity, a_i of the ions is unity, F, the Faraday's constant, R, the gas constant, and T, temperature. When the electrode potential is more negative (higher) than the energy level of vacant molecular orbital in the electrolyte solution, electrons will transfer from the electrode to the solution, accompanied by electrolyte reduction as shown in Fig. 1a. [30] If the electrode potential is more positive (lower) than the energy level of the occupied molecular orbital, the electrons will transfer from the electrolyte solution to the electrode, accompanied by electrolyte oxidation, as illustrated in Fig. 1b. [30] The reactions stop when the equilibrium is achieved.

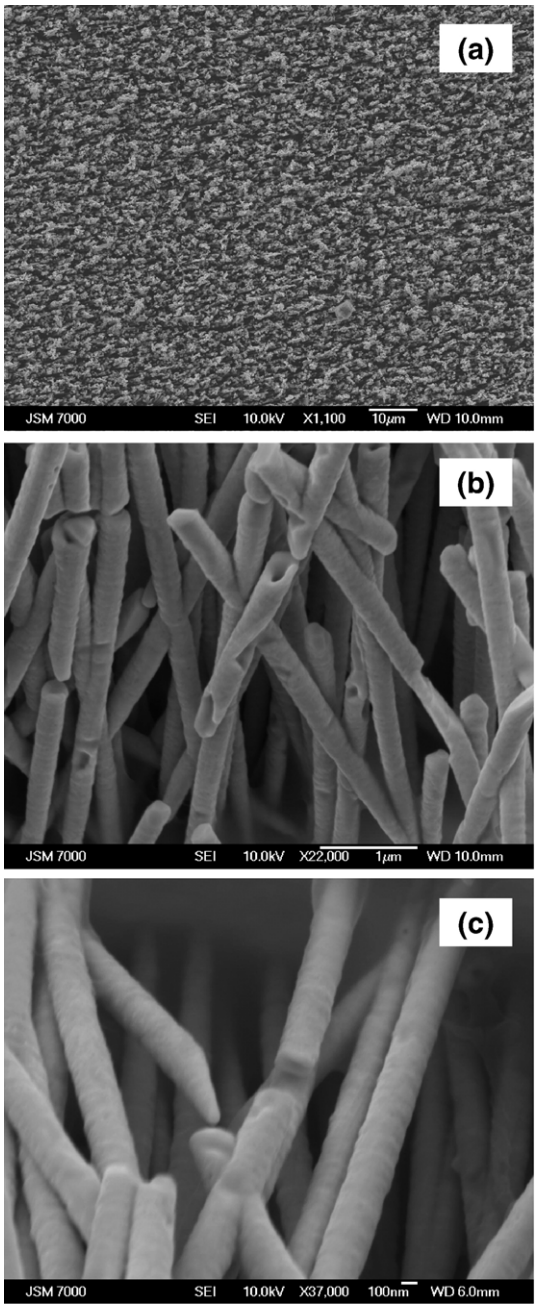

Fig. 3. SEM micrographs of (a) Au nanorod arrays grown in PC membranes covering a large area with uniform size and density, (b) Au nanotubes, ascribed to possible growth propagating along the surface of pore channels, and (c) Au nanorods, attributing to uniform growth from the bottom of pore channels attached to the electrode. [H.W. Wang, B. Russo, and G.Z. Cao, Nanotechnology 17 (2006) 2689].

When an external electric field is applied between two dissimilar electrodes, charged species flow from one to another electrode, and electrochemical reactions occur at both electrodes. This process is called electrolysis, which converts electrical energy to chemical potential. The system used for the electrolysis process is called electrolytic cell. In such a system the electrode connected to the positive side of the power supply is an anode, at which an oxidation reaction takes place, whereas the electrode connected to the negative side of the power supply is a cathode, at which a reduction reaction proceeds, accompanied by deposition. Therefore, electrolytic deposition is also called cathode deposition, but most commonly referred to as electrochemical deposition or electrodeposition.

The growth of nanowires of conductive materials in an electric field is a self-propagating process [31]. Once the small rods form, the electric field and the density of current lines between the tips of nanowires and the opposing electrode are greater than that between two electrodes due to a shorter distance. The growth species keep on depositing onto the tip of nanowires, resulting in continued growth. To better control the morphology and size, templates with desired channels are used to guide growth of nanowires. Fig. 2 illustrates the common set-up for the template-based growth of nanowires [32]. The template is attached onto the cathode, which is brought into contact with the deposition solution. The anode is placed in the deposition solution, parallel to the cathode. When an electric field is applied, cations diffuse through the channels toward and deposit on the cathode, resulting in the growth of nanowires inside the template. This figure also schematically shows the current density at different deposition stages when a constant electric field is applied. The current does not change significantly until the pores are completely filled, at which point the current increases rapidly due to the improved contact with the electrolyte solution. The current saturates once the template surface is completely covered.

3.1. Metals

A variety of metal nanowires, including Ni, Co, Cu and Au with nominal pore diameters between 10 and 200 nm have been synthesized by electrodeposition. For example, Possin [16] prepared various metallic nanowires using radiation track-etched mica. Likewise, Williams and Giordano [33] produced silver nanowires with diameters below 10 nm. Whitney et al. [32] fabricated the arrays of nickel and cobalt nanowires, also using PC templates. The growth of Au nanorod arrays have also been well studied [34,35]. Fig. 3 shows SEM micrographs of Au nanorod or nanowire arrays grown in templates by electrochemical deposition; both nanorod and nanotube arrays can be readily grown by varying the growth conditions, either to promote preferable growth along the surface of pore channels resulting in the formation of nanotube arrays, or to have deposition at the bottom of the pore channels attached to the electrode leading to the growth of nanorod arrays [36]. Single crystal bismuth nanowires have been grown in AAM using pulsed electrodeposition and Fig. 4 shows SEM and TEM images of the bismuth nanowires [36]. Single crystal copper and lead nanowires were prepared by DC electrodeposition and pulse electrodeposition, respectively [37,38]. The growth of single crystal lead nanowires required a greater departure from equilibrium conditions (greater over-potential) as compared with the conditions required for polycrystalline ones.

Hollow metal tubules can also be prepared [39,40]. In this case the pore walls of the template are chemically modified by anchoring organic silane molecules so that the metal will preferentially deposit onto the pore walls instead of the bottom electrode. For example, the pore surface of an anodic alumina template were first covered with cyanosilanes, subsequent electrochemical deposition resulted in the growth of gold tubules [41]. Surface modifying polymers can be directly added into the electrodeposition solution. For example, by adding a small amount of an amphiphilic triblock copolymer, pluronic P123 ($EO_{20}PO_{70}EO_{20}$, EO: ethylene oxide and PO: propylene oxide) in Ni electrodeposition solution, highly ordered arrays of Ni nanotube arrays were grown by electrodeposition [42]. The wall thickness of the nanotubes is uniform and can be controlled by the current density and the deposition time. Fig. 5 shows the TEM and SEM images of such grown Ni nanotube arrays after removal of anodic alumina membrane.

An electroless electrolysis process has also been investigated for the growth of nanowires and nanorods [21,40,43]. Electroless deposition is actually a chemical deposition process and involves the use of a chemical agent to coat a material onto the template surface [44]. The significant difference between

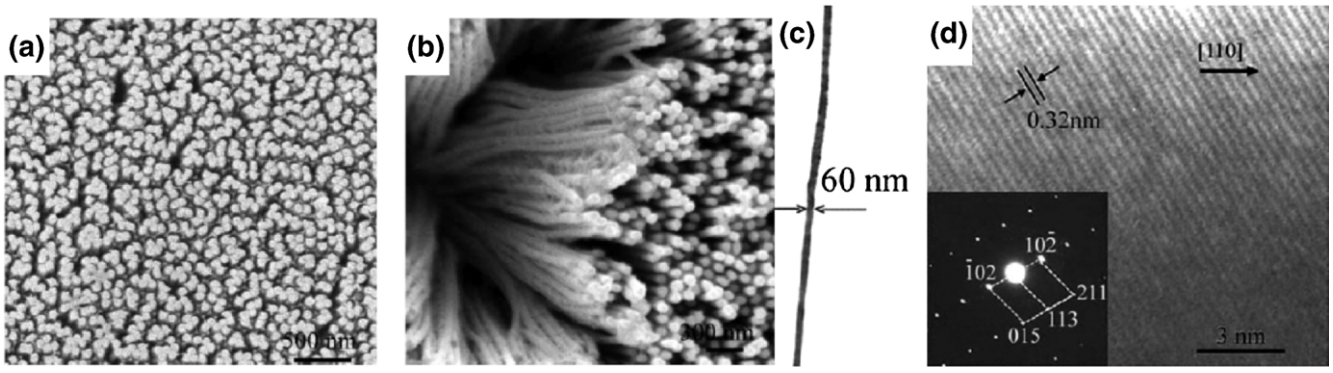

Fig. 4. SEM images of Bi nanowire arrays: (a) top view, (b) tilt view. (c) TEM image of a typical Bi single nanowire. (d) HRTEM image of a typical Bi single nanowire. The inset is the corresponding ED pattern. [C.G. Jin, G.W. Jiang, W.F. Liu, W.L. Cai, L.Z. Yao, Z. Yao and X.G. Li, J. Mater. Chem. 13 (2003) 1743].

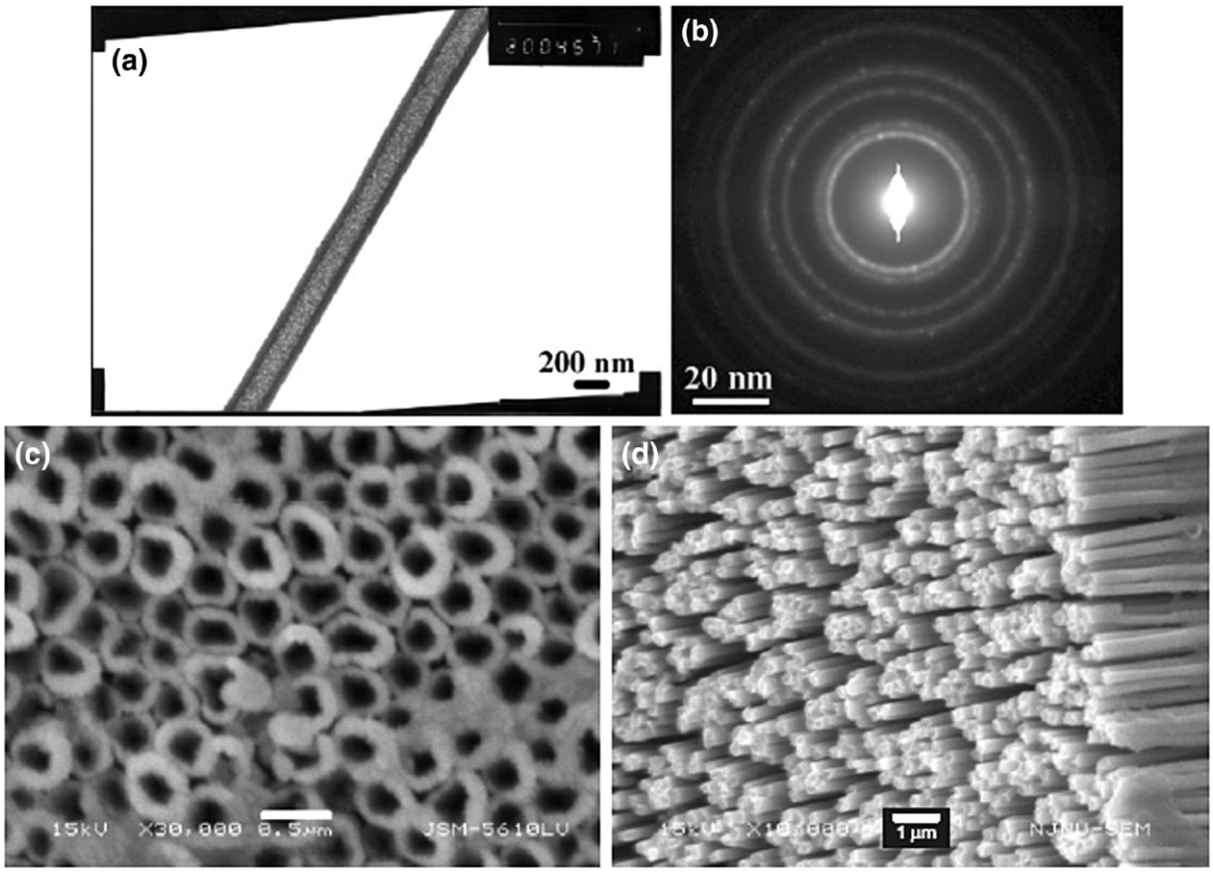

Fig. 5. a) TEM image and b) selected-area electron diffraction pattern of a Ni nanotube after completely removing the alumina template membrane. c) Top-view and d) side-view scanning electron microscopy images of an ordered-array of Ni nanotubes after partial removal of the alumina template membrane. The experimental parameters consisted of a current density of 0.13 $mAcm^{-2}$, a concentration of P123 of 37 $g\,L^{-1}$, and a deposition time of 48 h. [F.F. Tao, M.Y. Guan, Y. Jiang, J.M. Zhu, Z. Xu, and Z.L. Xue, Adv. Mater. 18 (2006) 2161].

electrochemical deposition and electroless deposition is that in the former, the deposition begins at the bottom electrode and the deposited materials must be electrically conductive. The electroless method does not require the deposited materials to be electrically conductive, and the deposition starts from the pore wall and proceeds inwardly. Therefore, in general, electrochemical deposition results in the formation of "solid" nanorods or nanowires of conductive materials, whereas the electroless deposition often grows hollow fibrils or nanotubules. For electrochemical deposition, the length of nanowires or nanorods can be controlled by the deposition time, whereas in electroless deposition the length of the nanotubules is solely dependent on the length of the deposition channels or pores. Variation of deposition time would result in a different wall thickness of nanotubules. An increase in deposition time leads to a thick wall, but sometimes the hollow tubule morphology persists even after a prolonged deposition.

Although many research groups have reported growth of uniformly sized nanorods and nanowires on PC template membranes, Schönenberger et al. [45] reported that the channels of carbonate membranes were not always uniform in diameter. They grew Ni, Co, Cu, and Au nanowires using polycarbonate membranes with nominal pore diameters between 10 and 200 nm by an electrolysis method. From both potentiostatic study of the growth process and SEM analysis of nanowire morphology, they concluded that the pores are in general not cylindrical with a constant cross-section, but are rather cigar-like. For the pores with a nominal diameter of 80 nm, the middle section of the pores is wider by up to a factor of 3. More recent work also found that the channels in PC membranes are not always parallel, instead there are a lot of cross-linked channels (as shown in Fig. 3a) [36].

3.2. Semiconductors

Semiconductor nanowire and nanorod arrays, were synthesized using AAM templates, such as CdSe and CdTe [46]. Nanowire arrays of bismuth telluride (Bi_2Te_3) can be used as a good example to illustrate the synthesis of compound nanowire arrays by electrochemical deposition. Bi_2Te_3 is of special interest as thermoelectric material and Bi_2Te_3 nanowire arrays are believed to offer higher figure of merit for thermal-electrical energy conversion [47,48]. Both polycrystalline and single crystal Bi_2Te_3 nanowire arrays have been grown by electrochemical deposition inside anodic alumina membranes [49,50]. Sander and co-workers [50] fabricated Bi_2Te_3 nanowire arrays with diameters as small as ~25 nm from a solution of 0.075 M Bi and 0.1 M Te in 1 M HNO_3 by electrochemical deposition at

−0.46 V vs Hg/Hg_2SO_4 reference electrode. The resultant Bi_2Te_3 nanowire arrays are polycrystalline in nature, and subsequent melting–recrystallization failed to produce single crystal Bi_2Te_3 nanowires. More recently, single crystal Bi_2Te_3 nanowire arrays have been grown from a solution consisted of 0.035 M $Bi(NO_3)_3 \cdot 5H_2O$ and 0.05 M $HTeO_2^+$; the latter was prepared by dissolving Te powder in 5 M HNO_3 by electrochemical deposition. Figs. 6 and 7 are the SEM image along with the XRD spectrum showing the cross-section of Bi_2Te_3 nanowire arrays and their crystal orientation. High resolution TEM and electron diffraction, together with XRD revealed that [110] is the preferred growth direction of Bi_2Te_3 nanowires. Single crystal nanowire or nanorod arrays can also be made through a careful control of the initial deposition [51]. Similarly, large area Sb_2Te_3 nanowire arrays have also been successfully grown by template-based electrochemical deposition, but the grown nanowires are polycrystalline and show no clear preferred growth direction [52].

Ultrasonication-assisted template-based electrodeposition has been demonstrated to be an effective approach for the synthesis of single crystalline nanorod arrays. For example, single crystalline *p*-type semiconductor copper sulfide nanorod arrays with diameter in the range of 50–200 nm and stoichiometric composition (Cu:S = 1:1) were synthesized through this method [53]. The electrolyte used was prepared by dissolving $Na_2S_2O_3$ (400 mM) and $CuSO_4$ (60 mM) in DI H_2O. Tartaric acid (75 mM) was used to maintain pH of the solution below 2.5. Liquid metal GaIn was used as the working electrode and a Pt spiral rod as a counter electrode. The electrodeposition of CuS was carried out at a constant electric potential and the entire electrochemical deposition cell was immersed in an ultrasonicator containing water. Fig. 8 shows the experimental results of the effects of ultrasonication on electrodeposition of CuS inside PC membranes. Fig. 8a compared the growth rates of electrodeposition under ultrasonication, stirring and regular (static) and revealed that ultrasonication significantly enhanced deposition process. Ultrasonication has also seen to result in an appreciable increase of the electrolyte temperature as shown in Fig. 8b. Fig. 8c revealed the current change when ultrasonication was switched on and off. A significantly high current indicates the lowered mass transfer resistance in the electrolyte solution [54].

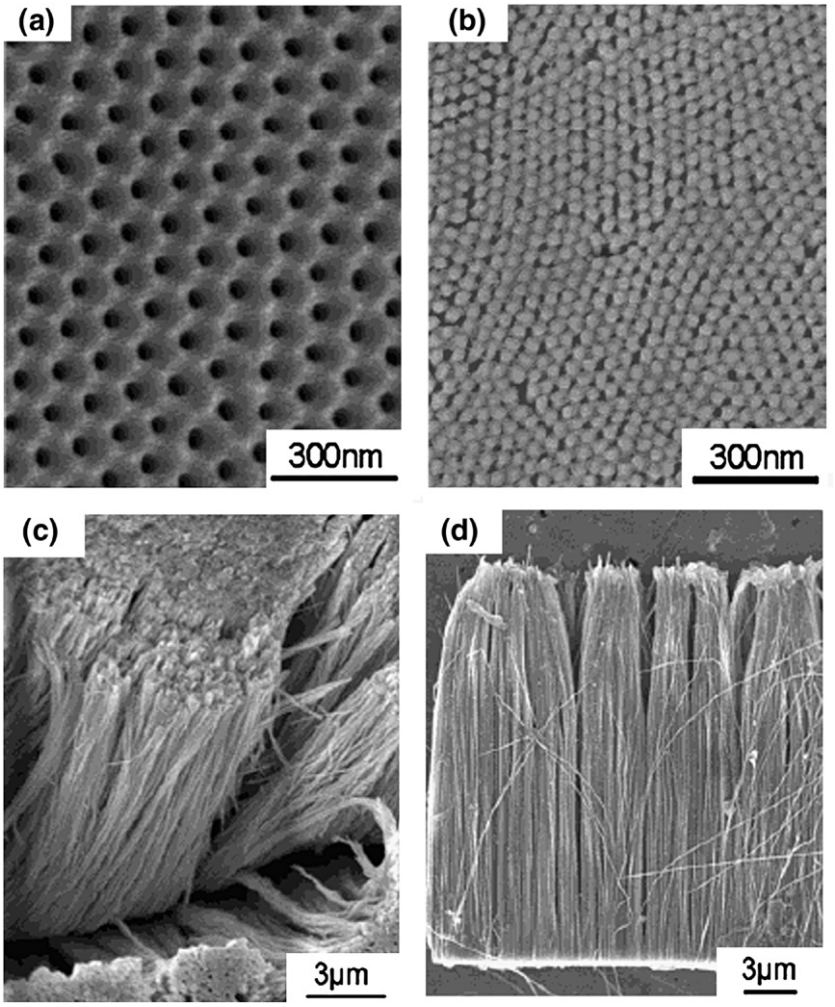

Fig. 6. SEM photographs of AAM template and Bi_2Te_3 nanowire arrays. (a) A typical SEM photograph of AAM. (b) Surface view of Bi_2Te_3 nanowire arrays (eroding time: 5 min). (c) Surface view of Bi_2Te_3 nanowire arrays (eroding time: 15 min). (d) Cross-sectional view of Bi_2Te_3 nanowire arrays (eroding time: 15 min). [C. Lin, X. Xiang, C. Jia, W. Liu, W. Cai, L. Yao, and X. Li, J. Phys. Chem. B108 (2004) 1844].

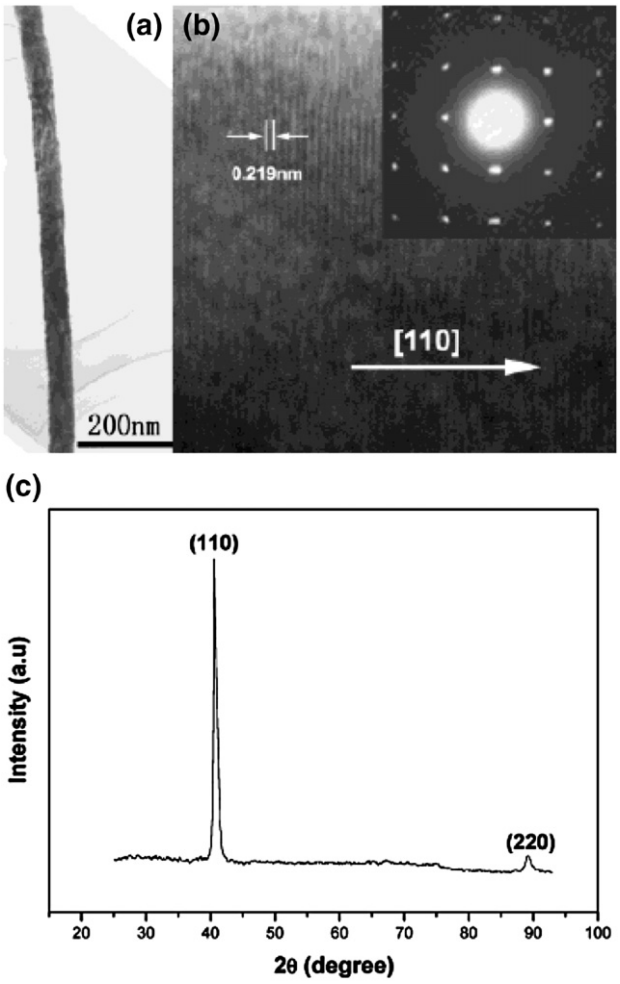

Fig. 7. TEM images and XRD pattern of a single Bi_2Te_3 nanowire. (a) TEM image and (b) HRTEM image of the same nanowire. The inset is the corresponding ED pattern. (c) XRD pattern of Bi_2Te_3 nanowire arrays (electrodeposition time: 5 min). [C. Lin, X. Xiang, C. Jia, W. Liu, W. Cai, L. Yao, and X. Li, J. Phys. Chem. B108 (2004) 1844].

3.3. Conductive polymers

Electrochemical deposition has also been explored for the synthesis of conductive polymer nanowire and nanorod arrays [55]. Conductive polymers have great potential for plastic electronics and sensor applications [56,57]. For example, Schönenberger et al. [46] have made conductive polypyrrole nanowires in PC membranes. Nanotubes are commonly observed for polymer materials as shown in Fig. 9 [58] in contrast to "solid" metal nanorods or nanowires. It seems that deposition or solidification of polymers insides template pores starts at the surface and proceeds inwardly. Martin [59] proposed to explain this phenomenon by the electrostatic attraction between the growing polycationic polymer and anionic sites along the pore walls of the polycarbonate membrane. In addition, although the monomers are soluble, the polymerized form is insoluble. Hence, there is a solvophobic component, leading to the deposition at the surface of the pores [60,61]. In the final stage, the diffusion of monomers through the inner pores becomes retarded and monomers inside the pores are quickly depleted. The deposition of polymer inside the inner pores stops.

Liang et al. [62] reported a direct electrochemical synthesis of oriented nanowires of polyaniline (PANI), a conducting polymer with its backbone conjugated by phenyl and amine groups, from solutions using no templates. The experimental design is on such basis that, in theory, the rate of electropolymerization (or nanowire growth) is related to the current density. Therefore, it is possible to control the nucleation and the polymerization rate by adjusting the current density. The synthesis involves electropolymerization of aniline ($C_6H_5NH_2$) and in-situ electrodeposition, resulting in nanowire growth.

3.4. Oxides

Similar to metals, semiconductors, and conductive polymers, some oxide nanorod arrays can be directly grown from solutions by electrochemical deposition. For example, V_2O_5 nanorod arrays have been grown on ITO substrate from $VOSO_4$ aqueous solution with VO^{++} as a growth species [63]. At the interface between the electrode (and subsequent growth surface) and electrolyte solution, the ionic cluster, VO^{+}, is oxidized and solid V_2O_5 is deposited through the following reaction.

$$2VO^{++} + 3H_2O \rightarrow V_2O_5 + 6H^{+} + 2e^{-} \quad (2)$$

A reduction reaction takes place at the counter electrode:

$$2H^{+} + 2e^{-} \rightarrow H_2(g) \quad (3)$$

It is obvious that pH and the concentration of VO^{++} clusters in the vicinity of the growth surface shift away from that in the bulk solution; both pH and VO^{++} concentration decrease.

Hydrous RuO_2 nanotube arrays were synthesized by means of template-assisted anodic deposition from an aqueous solution of 10 mM $RuCl_3$ and 0.1 M CH_3COONa [64]. Crystalline RuO_2 nanotube arrays were readily obtained by annealing at elevated temperatures. ZnO nanowire arrays were fabricated by one-step electrochemical deposition technique based on ordered nanoporous alumina membrane [65]. ZnO nanowire array is uniformly assembled into the nanochannels of anodic alumina membranes and consists of single crystal particles.

4. Electrophoretic deposition

The electrophoretic deposition technique has been widely explored, particularly for deposition of ceramic and organoceramic materials on cathode from colloidal dispersions [66–68]. Electrophoretic deposition differs from electrochemical deposition in several aspects. First, the deposit by electrophoretic deposition method needs not to be electrically conductive. Secondly, nanosized particles in colloidal dispersions are typically stabilized by electrostatic or electrosteric mechanisms. As discussed in the previous section, when dispersed in a polar solvent or an electrolyte solution, the surface of nanoparticles develops an electrical charge via one or more of the

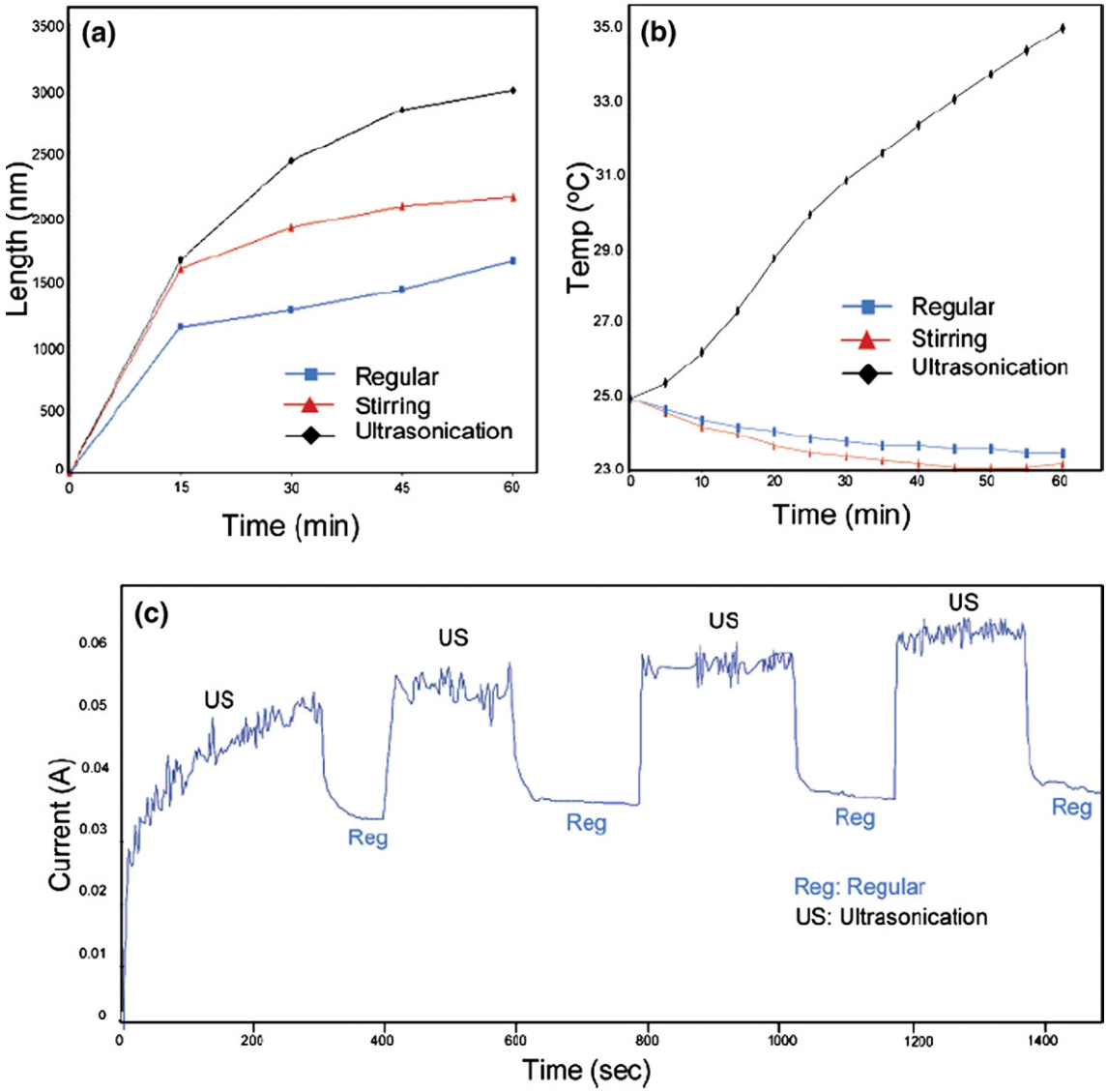

Fig. 8. Effect of ultrasonication on electrodeposition. (a) Growth rate of nanorods for ultrasonication, stirring, and regular processes. (b) Temperature rate of bulk electrolyte for same three processes. (c) Effect on resistance provided to electrodeposition by "ultrasonication". [K.V. Singh, A.A. Martinez-Morales, G.T.S. Andavan, K.N. Bozhilov, and M. Ozkan, Chem. Mater. 19 (2007) 2446].

following mechanisms: (1) preferential dissolution, (2) deposition of charges or charged species, (3) preferential reduction or oxidation, and (4) physical adsorption of charged species such as polymers. A combination of electrostatic forces, Brownian motion and osmotic forces would result in the formation of a so-called double layer structure, schematically illustrated in Fig. 10. The figure depicts a positively charged particle surface, the concentration profiles of negative ions (counter-ions) and positive ions (surface-charge-determining-ions), and the electric potential profile. The concentration of counter-ions gradually decreases with distance from the particle surface, whereas that of charge-determining ions increases. As a result, the electric potential decreases with distance. Near the particle surface, the electric potential decreases linearly, in the region known as the Stern layer. Outside of the Stern layer, the decrease follows an exponential relationship. The region between Stern layer and the point where the electric potential equals zero is called the diffusion layer. Together, the Stern layer and diffusion layer are called the double layer structure in the classic theory of electrostatic stabilization.

Upon application of an external electric field, charged particles are set in motion as schematically illustrated in Fig. 11 [1]. This type of motion is referred to as electrophoresis. When a charged particle moves, some of the solvent or solution surrounding the particle will also move with it, since part of the solvent or solution is tightly bound to the particle. The plane that separates the tightly bound liquid layer from the rest of the liquid is called the slip plane (Fig. 10). The electric potential at the slip plane is known as the zeta potential, which is an important parameter in determining the stability and transport of a colloidal dispersion or a sol. A zeta potential larger than about 25 mV is typically required to stabilize a system [69]. The

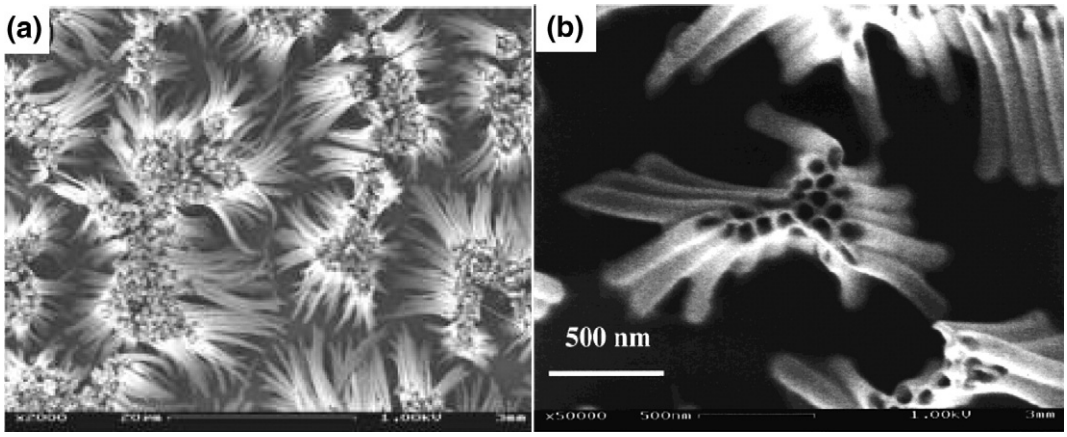

Fig. 9. SEM images of polymer nanotubes, indicating the fact that deposition or solidification of polymers insides template pores preferably starts at the surface of pore channels and proceeds inwardly. [L. Dauginet, A.-S. Duwez, R. Legras, and S. Demoustier-Champagne, Langmuir, 17 (2001) 3952].

zeta potential, ζ, around a spherical particle can be described as [70]:

$$\zeta = \frac{Q}{4\pi\varepsilon_r a(1+\kappa a)} \tag{4}$$

with $\kappa = \left(\frac{e^2\sum n_i z_i^2}{\varepsilon_r\varepsilon_0 kT}\right)^{1/2}$ where Q is the charge on the particle, a is the radius of the particle out to the shear plane, ε_r is the relative dielectric constant of the medium, and n_i and z_i are the bulk concentration and valence of the ith ion in the system, respectively.

The mobility of a nanoparticle in a colloidal dispersion or a sol, μ, is dependent on the dielectric constant of the liquid medium, ε_r, the zeta potential of the nanoparticle, ζ, and the viscosity, η, of the fluid. Several forms for this relationship have been proposed, such as the Hückel equation [71–74]:

$$\mu = \frac{2\varepsilon_r\varepsilon_0\zeta}{3\pi\eta} \tag{5}$$

Electrophoretic deposition simply uses oriented motion of charged particles in a electrical field to grow films or monoliths by enriching the solid particles from a colloidal dispersion or a sol onto the surface of an electrode. If particles are positively charged (more precisely speaking, having a positive zeta potential), the deposition of solid particles will occur at the cathode. Otherwise, deposition will be at the anode. At the electrodes, the electrostatic double layers collapse and the particles coagulate, producing a porous materials made of compacted nanoparticles.

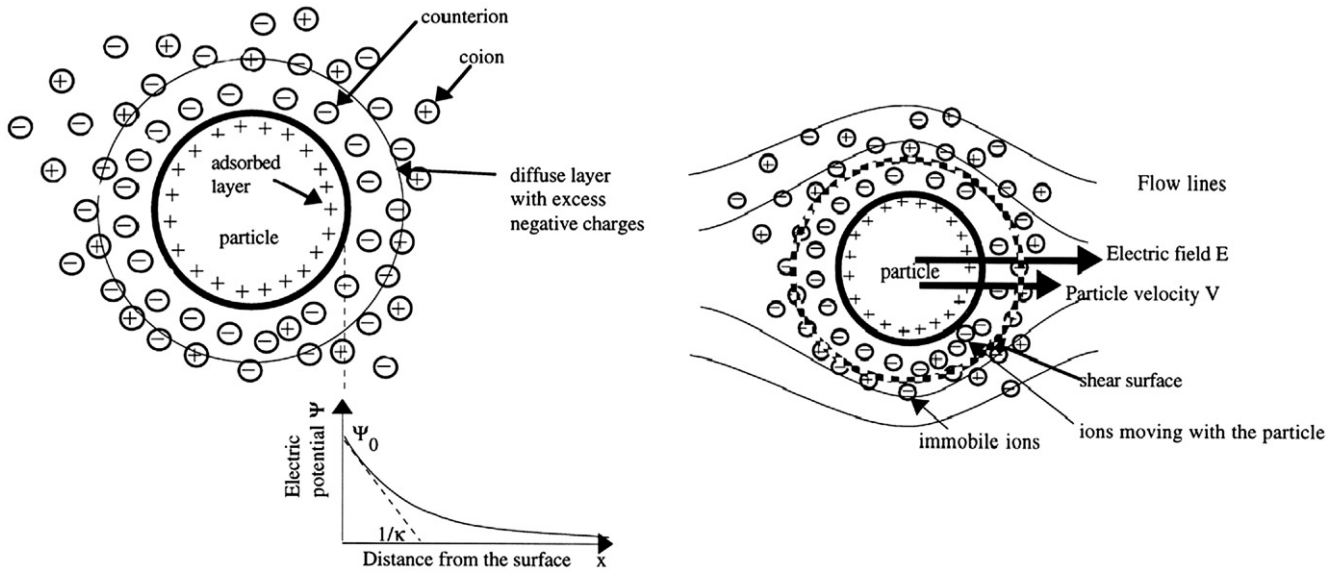

Fig. 10. Schematic illustrating electrical double layer structure and the electric potential near the solid surface with both Stern and Gouy layers indicated. Surface charge is assumed to be positive. [A.C. Pierre, Introduction to Sol–Gel Processing, Kluwer, Norwell, MA, 1998.].

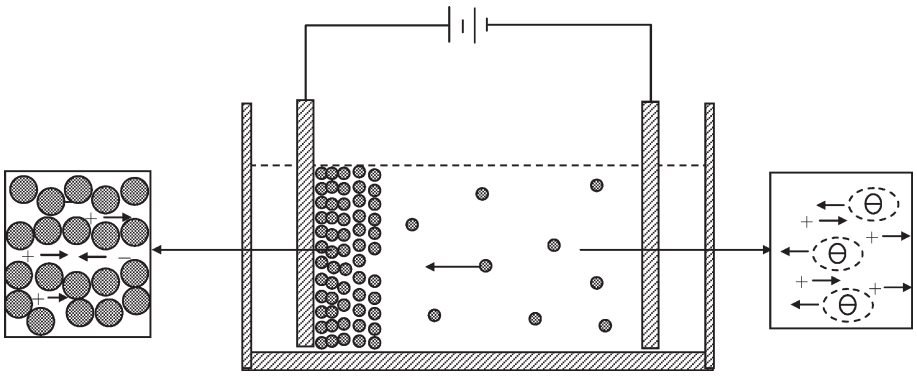

Fig. 11. Schematic showing the electrophoresis. Upon application of an external electric field to a colloidal system or a sol, the constituent charged nanoparticles or nanoclusters are set in motion in response to the electric field. [G.Z. Cao, Nanostructures and Nanomaterials: Synthesis, Properties and Applications, Imperial College Press, London, UK, 2004].

Typical packing densities are far less than the 74 vol.% theoretical density [75]. Many theories have been proposed to explain the processes at the deposition surface during electrophoretic deposition. However, the structural evolution on the growth surfaces is not well understood. Electrochemical process at the deposition surface or electrodes is complex and varies from system to system. The final density is dependent on the concentration of particles in sols or colloidal dispersions, zeta potential, externally applied electric field, and reaction kinetics between particle surfaces. Slow reaction and slow arrival of

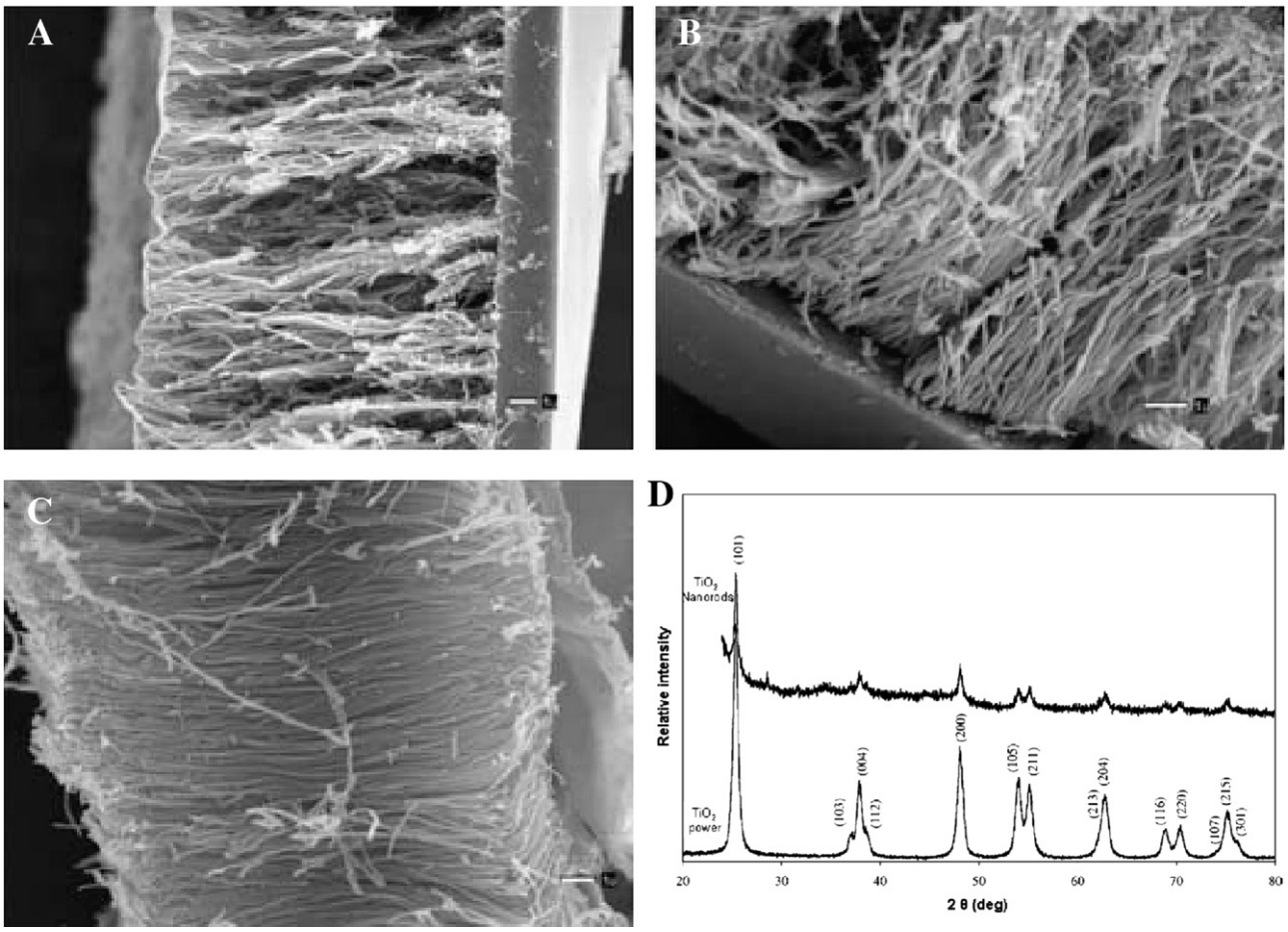

Fig. 12. SEM micrograph of TiO_2 nanorod arrays grown by template-based sol electrophoretic deposition. The diameters of nanorods are approximately: (A) 180 nm (for the 200 nm polycarbonate membrane), (B) 90 nm (for the 100 nm membrane), (C) 45 nm (for the 50 nm membrane) and (D) XRD patterns of both the grown nanorods and a powder derived from the same sol, and both samples consist of the anatase phase only and no peak position shift was observed. [S.J. Limmer, T.P. Chou, G.Z. Cao, J. Mater. Sci. 39 (2004) 895].

nanoparticles onto the surface would allow sufficient particle relaxation on the deposition surface, so that a high packing density is expected.

4.1. Polycrystalline oxides

Limmer et al. [76–82] combined sol–gel preparation with electrophoretic deposition to prepare nanorods of various complex oxides. One of the advantages of this technique is the ability to synthesize complex oxides and organic–inorganic hybrids with desired stoichiometric composition. Another advantage is the applicability to a variety of materials. In their approach, conventional sol–gel processing was applied to the synthesis of various sols. By appropriate control of the sol preparation, nanometer particles with desired stoichiometric composition were formed, and electrostatically stabilized by pH adjustment. Using radiation tracked etched polycarbonate membranes with an electric field of ~1.5 V/cm, they have grown nanowires with diameters ranging from 40 to 175 nm and a length of 10 μm, corresponding to the thickness of the membrane. The materials include anatase TiO_2, amorphous SiO_2, perovskite $BaTiO_3$ and $Pb(Ti,Zr)O_3$, and layered perovskite $Sr_2Nb_2O_7$. Fig. 12 shows the SEM micrographs and XRD patterns of TiO_2 nanorod arrays [80].

Wang et al. [83] used electrophoretic deposition to make nanorods of ZnO from colloidal sols. ZnO colloidal sol was prepared by hydrolyzing an alcoholic solution of zinc acetate with NaOH, with a small amount of zinc nitrate added as a binder. This solution was then introduced into the pores of anodic alumina membranes at voltages in the range of 10–400 V. It was found that lower voltages led to dense, solid nanorods, while higher voltages caused the formation of hollow tubules. They suggested that the higher voltages cause dielectric breakdown of the anodic alumina, causing it to become positively charged as the cathode. Electrostatic attraction between the ZnO nanoparticles and the pore walls then leads to tubule formation.

4.2. Single crystal oxide nanorod arrays by change of local pH

A modified version of sol electrophoretic deposition has been demonstrated to be capable of growing single crystalline titanium oxide and vanadium pentoxide nanorod arrays from respective TiO^{2+} and VO_2^+ solutions. Miao et al. [84] prepared single crystalline TiO_2 nanowires by electrochemically induced sol–gel deposition. Titania electrolyte solution was prepared by dissolving Ti powder into a H_2O_2 and NH_4OH aqueous solution to form TiO^{2+} ionic clusters [85]. When an electric field was applied, TiO^{2+} ionic clusters diffused to the cathode and underwent hydrolysis and condensation reactions, resulting in deposition of nanorods of amorphous TiO_2 gel. After heating at 240 °C for 24 h in air, single crystal anatase nanorods with diameters of 10, 20, and 40 nm, and lengths ranging from 2 to 10 μm, were synthesized. The formation of single crystal TiO_2 nanorods here is different from that reported by Martin's group [86]. It is suggested that the nanoscale crystallites generated during heating assembled epitaxially to form single crystal nanorods.

In a typical sol–gel processing, nanoclusters are formed through homogeneous nucleation and subsequent growth through sequential yet parallel hydrolysis and condensation reactions. Sol electrophoretic deposition is to enrich and deposit such formed nanoclusters at an appropriate electrode surface under an external electric field. The modified process is to limit and induce the condensation reaction at the growth surface through the change of local pH value, which is a result of partial water hydrolysis at the electrode or growth surface:

$$2H_2O + 2e^- \rightarrow H_2 + 2OH^- \quad (6)$$

$$2VO_2^+ + 2OH^- \rightarrow V_2O_5 + H_2O \quad (7)$$

Reaction 6, or the electrolysis of water, plays a very important role here. As the reaction proceeds, hydroxyl groups are produced, resulting in an increased pH at the proximity of the deposition surface. Such an increase of pH value near to the growth surface initiated and promoted the precipitation of V_2O_5, or reaction 7. The initial pH of VO_2^+ solution is approximately 1.0, in which VO_2^+ is stable. However, when pH increases to ~1.8, VO_2^+ is no longer stable and solid V_2O_5 would form. Since the change of pH occurs at the proximity of the growth surface, reaction 7 or deposition is likely to occur on

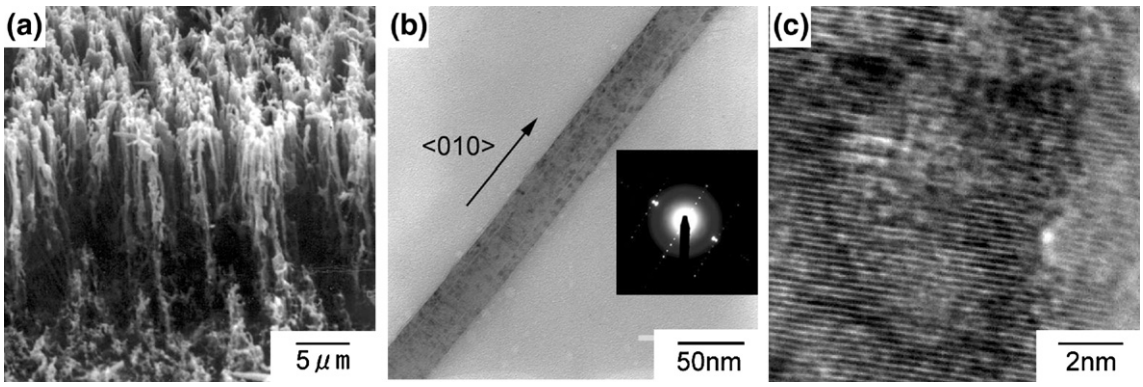

Fig. 13. (a) SEM image of V_2O_5 nanorod arrays on an ITO substrate grown in a 200 nm carbonate membrane by sol electrophoretic deposition, (b) TEM image of a V_2O_5 nanorod with its electron diffraction pattern, and (c) high resolution TEM image of the V_2O_5 nanorod showing the lattice fringes. [K. Takahashi, S.J. Limmer, Y. Wang, and G.Z. Cao, Jpn. J. Appl. Phys. B44 (2005) 662].

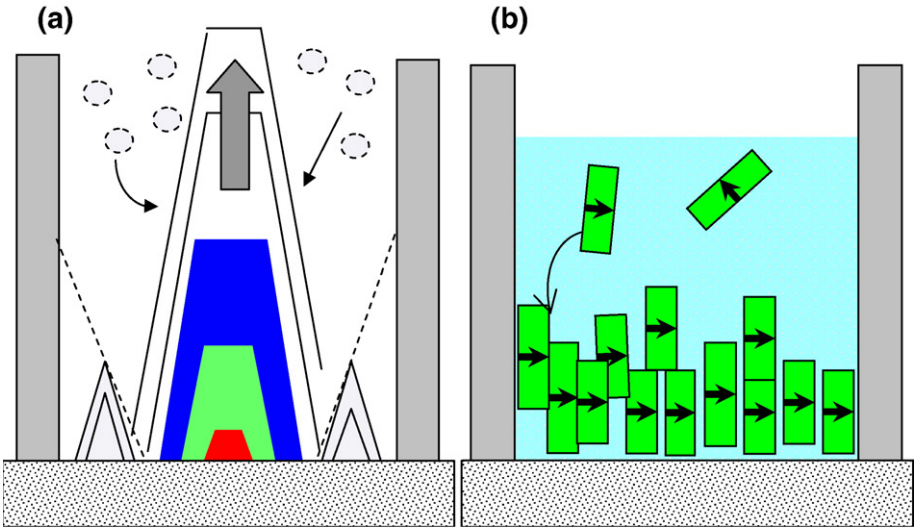

Fig. 14. Schematic illustrations of (a) the mechanism of evolution selection growth inside a pore channel leading to the formation of single crystal nanorod (left) and (b) homoepitaxial aggregation growth mechanism of a single crystalline nanorod (right). [G.Z. Cao, J. Phys. Chem. B108 (2004) 19921].

the surface of the electrode through heterogeneous nucleation and subsequent growth. It should be noted that the hydrolysis of water has another influence on the deposition of solid V_2O_5. Reaction 6 produces hydrogen on the growth surface. Such molecules may poison the growth surface before dissolving into the electrolyte or forming a gas bubble, which may cause the formation of porous nanorods.

The formation of single crystal nanorods from solutions by pH change induced surface condensation has been proven by TEM analyses including high resolution image showing the lattice fringes and electron diffraction. Fig. 13 shows typical SEM and TEM micrographs and selected-area electron diffraction pattern of V_2O_5 nanorods. It is well known that [010] or *b*-axis is the fastest growth direction for V_2O_5 crystal [87,88], which would explain why single crystal vanadia nanorods or a bundle of single crystal nanorods grow along the b-axis. The growth of single crystal nanorods by pH change induced surface condensation is attributed to evolution selection growth, which is briefly summarized below and illustrated in Fig. 14a. The initial heterogeneous nucleation or deposition on the substrate surface results in the formation of nuclei with random orientation. The subsequent growth of various facets of a nucleus is dependent on the surface energy, and varies significantly from one facet to another [89]. For one-dimensional growth, such as film growth, only the highest growth rate with direction perpendicular to the growth surface will be able to continue to grow. The nuclei with the fastest growth direction perpendicular to the growth surface will grow larger, while nuclei with slower growth rate will eventually cease to grow. Such growth mechanism would result in the formation of columnar structured films with all the grains having the same crystal orientation (known as textured films) [90,91]. In the case of nanorod growth inside a pore channel, such evolution selection growth is likely to lead to the formation of a single crystal nanorod or a bundle of single crystal nanorods per pore channel.

4.3. Single crystal oxide nanorod arrays by homoepitaxial aggregation

Single crystal nanorods can also grown directly by conventional electrophoretic deposition. However, several requirements have to be met for such growth. First, the nanoclusters or particles in the sol must have a crystalline structure extended to the surface. Second, the deposition of nanoclusters on the growth must have a certain degree of reversibility so that the nanoclusters can rotate or re-position prior to its irreversible incorporation into the growth surface. Thirdly, the deposition rate must be slow enough to permit sufficient time for the nanoclusters to rotate or re-positioning. Lastly, the surface of nanoclusters must be free of strongly attached alien chemical species. Although precise control of all these parameters remains a challenge, the possibility of growth of single crystal nanorods through homoepitaxial aggregation of nanocrystals has been demonstrated [92,93]. The formation of single crystalline vanadium pentoxide nanorods by template-based sol electrophoretic deposition can be attributed to homoepitaxial aggregation of crystalline nanoparticles. Thermodynamically it is favorable for the crystalline nanoparticles to aggregate epitaxially; such growth behavior and mechanism have been well documented in literature [94,95]. In this growth mechanism, initial weak interaction between two nanoparticles allows rotation and migration relative to each other. Obviously, homoepitaxial aggregation is a competitive process and porous structure is expected to form through such homoepitaxial aggregation (as schematically illustrated in Fig. 14b). Vanadium oxide particles in a typical sol are known to form ordered crystalline structure easily [96], so that it is reasonable to expect that homoepitaxial aggregation of vanadia nanocrystals from sol results in the formation of single crystal nanorods. Such formed single crystal nanorods are likely to undergo significant shrinkage when fired at high temperatures due to its original porous nature; 50% lateral shrinkage has been observed in

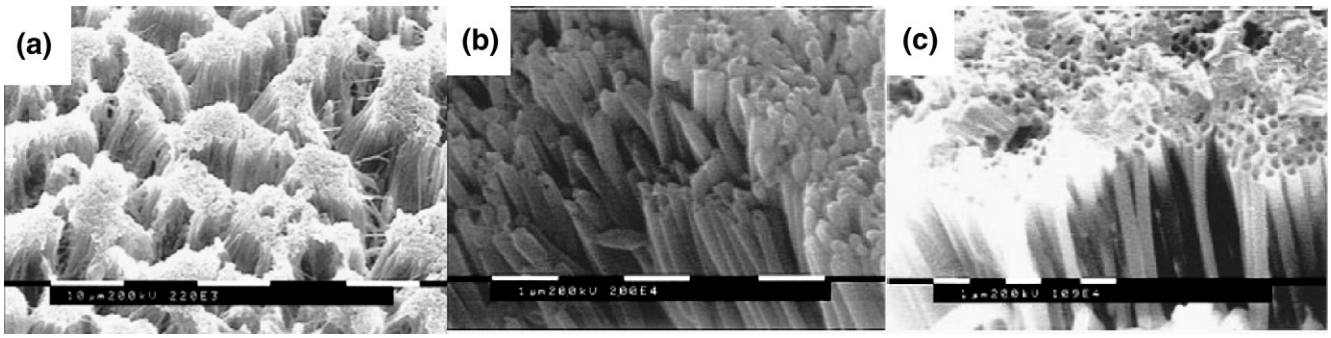

Fig. 15. SEM micrographs of oxide nanorods made by simple filling the templates with sols: a) ZnO, b) TiO_2 and c) hollow nanotube. [B.B. Lakshmi, P.K. Dorhout, and C.R. Martin, Chem. Mater. 9 (1997) 857].

vanadium pentoxide nanorods formed by this method. In addition, it might be possible that the electric field and the internal surface of pore channels both play a significant role in the orientation of nanorods, as suggested in literature [97,98].

4.4. Nanowires and nanotubes of fullerenes and metallofullerenes

Electrophoretic deposition in combination with template-based growth has also been successfully explored for the formation of nanowires and nanotubes of carbon fullerenes, such as C_{60} [99], or metallofullerenes, $Sc@C_{82}(I)$ [100]. Typical experiments include purification or isolation of desired fullerenes or metallofullerenes using multiple step liquid chromatography and dispersion the fullerenes in a mixed solvent of acetonitrile/toluene in a ratio of 7:1. The electrolyte solution has a relatively low concentration of fullerenes (35 μm) and metallofullerenes (40 μm), and the electrophoretic deposition took place with an externally applied electric of 100–150 V with a distance of 5 mm set between two electrodes. Both nanorods and nanotubes of fullerenes or metallofullerenes can be formed and it is believed that the initial deposition occurred along the pore surface. Short deposition time would result in the formation of nanotubes, whereas extended deposition leads to the formation of solid nanorods. Such formed nanorods can possess either crystalline or amorphous structure.

5. Template filling

Direct template filling from a liquid precursor of mixture is the most straightforward and versatile method for preparing nanowire or nanorod arrays. The drawback of this approach is the difficult to ensure complete filling of the template pores. Both nanorods and nanotubules can be obtained depending on the interfacial adhesion and the solidification modes. If the adhesion between the pore walls and the filling material is weak, or solidification starts at the center (or from one end of the pore, or uniformly throughout the rods), solid nanorods are likely to form. If the adhesion is strong, or the solidification starts at the interfaces and proceeds inwardly, hollow nanotubules are likely to form.

5.1. Colloidal dispersion filling

Martin et al. [87,101] have studied the formation of various oxide nanorods and nanotubules by simply filling the templates with colloidal dispersions (Fig. 15). Recently, the mesoporous material (SBA-15) nanorod arrays were synthesized by filling the sol containing surfactant (Pluronic P123) inside an ordered porous alumina membrane [102]. Colloidal dispersions were prepared using appropriate sol–gel processing techniques. The template was placed in a stable sol for various period of time. The capillary force drives the sol into the pores if the sol has good wettability for the template. After the pores were filled with sol, the template was withdrawn from the sol and dried. The sample was fired at elevated temperatures to remove template and to densify the sol–gel-derived green nanorods.

Typically a sol consists of a large volume fraction of solvent, up to 90% or higher. Although the capillary force may ensure complete filling of the pores with the suspension, the amount of the solid occupying the pore space is small. Upon drying and subsequent firing processes, a significant shrinkage would be expected. However, the actual shrinkage observed is small when compared with the pore size. These results indicated that there are some unknown mechanisms, which enrich the concentration of solid inside pores. One possible mechanism could be the diffusion of solvent through the membrane, leading to the enrichment of solid along the internal surface of template pores, similar to what happens during ceramic slip casting [70]. The observation of formation of nanotubules (as shown in Fig. 15 [87]) may imply that such a process is indeed present. However,

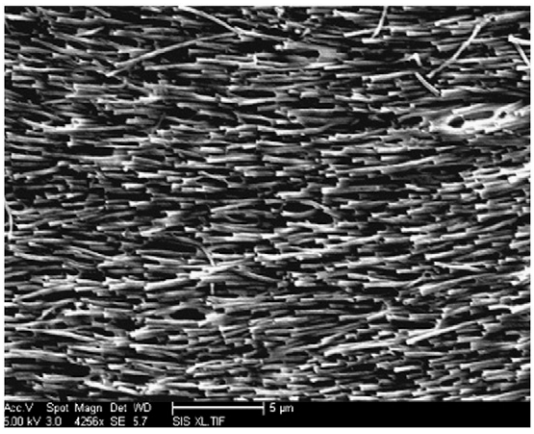

Fig. 16. Nanofiber arrays of biodegradable polymers, PCL, by bringing porous template in contact with the polymer melt when heated at 130 °C. [S.L. Tao, and T.A. Desai, Nano Lett. 7 (2007) 1463].

considering the fact that the templates typically were emerged into sol for just a few minutes, the diffusion through membrane and enrichment of solid inside the pores must be a rather rapid process. It is also noticed that the nanorods made by template filling are commonly polycrystalline or amorphous, but sometimes single crystal TiO_2 nanorods were observed for nanorods smaller than 20 nm [87].

Supercritical-fluid-inclusion is an ideal method for the formation of high density arrays of nanowires within AAO templates as they do not suffer from the inherent problem of pore blocking associated with other methods such as electrodeposition. For example, high density Ge nanowire arrays were synthesized by this method [103].

5.2. Melt and solution filling

Metallic nanowires can also be synthesized by filling a template with molten metals [104]. One example is the preparation of bismuth nanowires by pressure injection of molten bismuth into the nanochannels of an anodic alumina template [105]. The anodic alumina template was degassed and immersed in the liquid bismuth at 325 °C (T_m=271.5 °C for Bi), and then high pressure Ar gas of ~300 bar was applied to inject liquid Bi into the nanochannels of the template for 5 h. Bi nanowires with diameters of 13–110 nm and large aspect ratios up to several hundred have been obtained. Individual nanowires are believed to be single crystal. When exposed to air, bismuth nanowires are readily oxidized. An amorphous oxide layer of ~4 nm in thickness was observed after 48 h. After 4 weeks, the bismuth nanowires were completely oxidized. Nanowires of other metals, such as In, Sn, and Al, and semiconductors, Se, Te, GaSb, and Bi_2Te_3, were also prepared by injection of molten liquid into anodic alumina templates [106].

Polymeric fibrils have been made by filling a monomer solution containing the desired monomer and a polymerization reagent into the template pores, followed by in-situ polymerization [19,107–110]. The polymer preferentially nucleates and grows on the pore walls, resulting in tubules at short deposition times. Biodegradable poly(ε-caprolactone) (PCL) nanofibers was fabricated by extrusion of a precursor solution through a template and solidifying under pressure [111]. Alternately PCL nanofibers were synthesized by bringing porous template in contact with the polymer melt when heated at 130 °C [112] and the well controlled PCL nanorod arrays are shown in Fig. 16. This latter method is solvent-free and low temperature fabrication process and would also offer better control of nanostructures. However, this approach requires a good wettability between the pore surface of templates and the melts. When polymer powder was first filled into the pores of template membrane and then melt inside the pores, nanotube arrays with well defined wall thickness would form with good wetting of polymer melt on the pore surface [113]. The formation of nanotube arrays instead of nanorod arrays in the latter is simply due to limited available polymer melts inside the pores as powder would not fill up the entire space.

Recently, metal, oxide and semiconductor nanowires have been synthesized using self-assembled mesoporous silica as the template. For example, Han et al. [114] have synthesized Au, Ag and Pt nanowires in mesoporous silica templates. The mesoporous templates were first filled with aqueous solutions of the appropriate metal salts (such as $HAuCl_4$). After drying and treatment with CH_2Cl_2, the samples were reduced under H_2 flow to form metallic nanowires. Liu et al. [115] carefully studied the interface between these nanowires and the matrix using high resolution electron microscopy and electron energy loss spectroscopy techniques. A sharp interface only exists between noble metal nanowires and the matrix. For magnetic nickel oxide, a core shell nanorod structure containing a nickel oxide core and a thin nickel silicate shell was observed. The magnetic properties of the templated nickel oxide were found to be significantly different from nickel oxide nanopowders due to the alignment of the nanorods. In another study, Chen et al filled the pores of a mesoporous silica template with an aqueous solution of Cd and Mn salts, dried the sample, and reacted it with H_2S gas to convert to (Cd,Mn)S [116].

Mesoporous silica has been grown inside porous channels of anodic alumina and PC membranes. Petkov et al [117] has grown mesoporous silica from tetraethyl orthosilicate (TEOS)

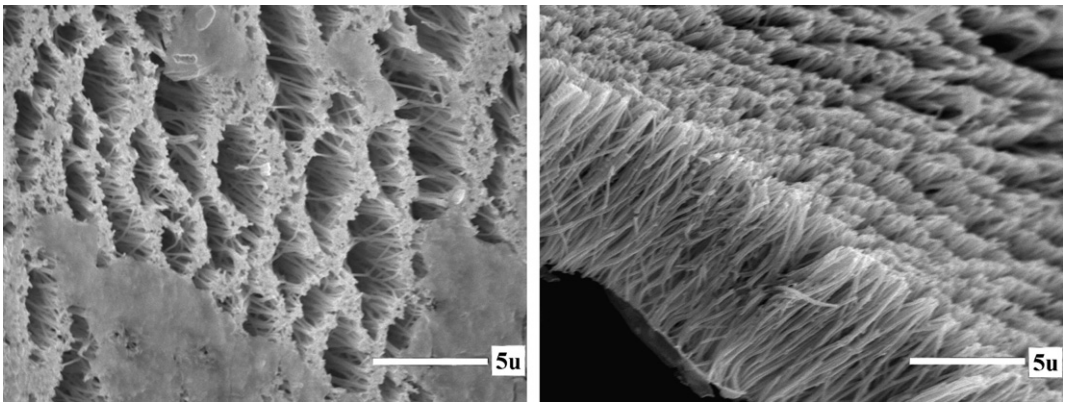

Fig. 17. SEM images of the top view (left) and side view (right) of lead zirconate titanate (PZT) nanorod arrays grown in polycarbonate membrane from PZT sol by centrifugation at 1500 rpm for 60 min. Samples were attached to silica glass and fired at 650 °C in air for 60 min. [T.L. Wen, J. Zhang, T.P. Chou, and G.Z. Cao, J. Sol–gel. Sci. Technol. 33 (2005) 193].

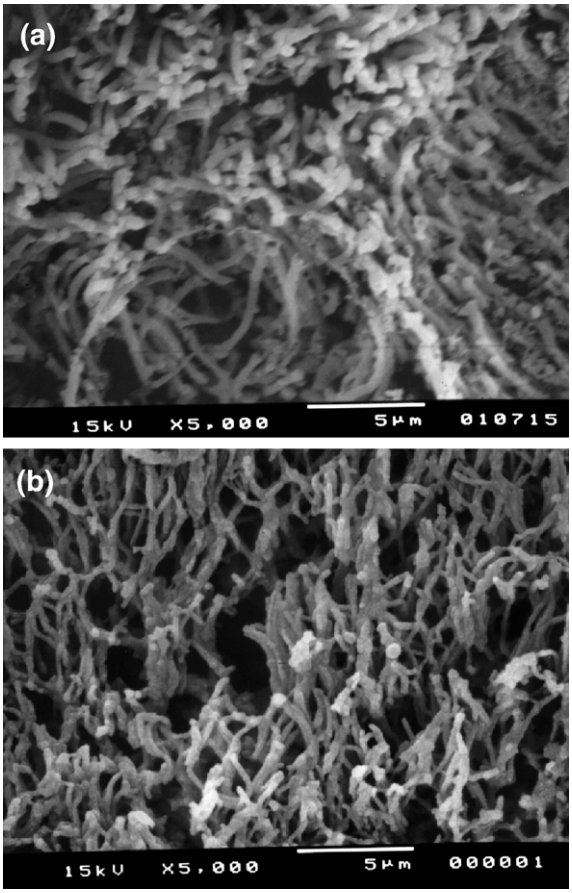

Fig. 18. SEM images of (a) pure V_2O_5 nanorods grown in PC membranes with 400-nm-diameter pores using capillary force induced filling and solvent evaporation induced deposition method and fired at 485 °C and (b) V_2O_5–TiO_2 (molar ratio V/Ti = 50/50) composite nanorod arrays. [K. Takahashi, Y. Wang, K.H. Lee, and G.Z. Cao, Appl. Phys. A82 (2006) 27].

as the silica precursor and poly(ethylene oxide)-b-poly(propylene oxide)-b-poly(ethylene oxide) triblock copolymer, Pluronic-123 as templating molecule. First a pre-hydrolyzed silica sol was prepared by mixing TEOS with ethanol, water, and hydrogen chloride at 60 °C for 1 h, and then admixed with Pluronic 123 dissolved in ethanol. NH_4Cl was then added to ensure the complete dissolution of inorganic salt. Anodic alumina membrane was then soaked into such a triblock copolymer silica sol at room temperature for 2 h. The membrane was then dried and calcined in flowing air at 550 °C for 5 h. Mesopore channels in mesoporous silica are parallel to the pore channels in alumina membranes. Such mesoporous silica in anodic alumina membranes were used to grow metal and semiconductor nanowires inside the mesopores in silica. Limmer et al [118] has grown mesoporous silica arrays by means of sol electrophoretic deposition using surfactant containing silica sol and PC membrane as templates.

5.3. Centrifugation

Template filling of nanoclusters assisted with centrifugation forces is another inexpensive method for mass production of nanorod arrays. Fig. 17 shows SEM images of lead zirconate titanate (PZT) nanorod arrays with uniformly sizes and unidirectional alignment [119]. Such nanorod arrays were grown in polycarbonate membrane from PZT sol by centrifugation at 1500 rpm for 60 minutes. The samples were attached to silica glass and fired at 650 °C in air for 60 min. Nanorod arrays of other oxides (silica and titania) have prepared. The advantages of centrifugation include its applicability to any colloidal dispersion systems, including those consisting of electrolyte-sensitive nanoclusters or molecules.

5.4. Solvent evaporation induced deposition

Although many elegant techniques have been developed for the synthesis of oxide nanorod arrays from colloidal dispersions as discussed above, many of them can not be used for growing composite nanorod arrays. For example, sol electrophoretic deposition can be used to prepare single-phase nanorod arrays;

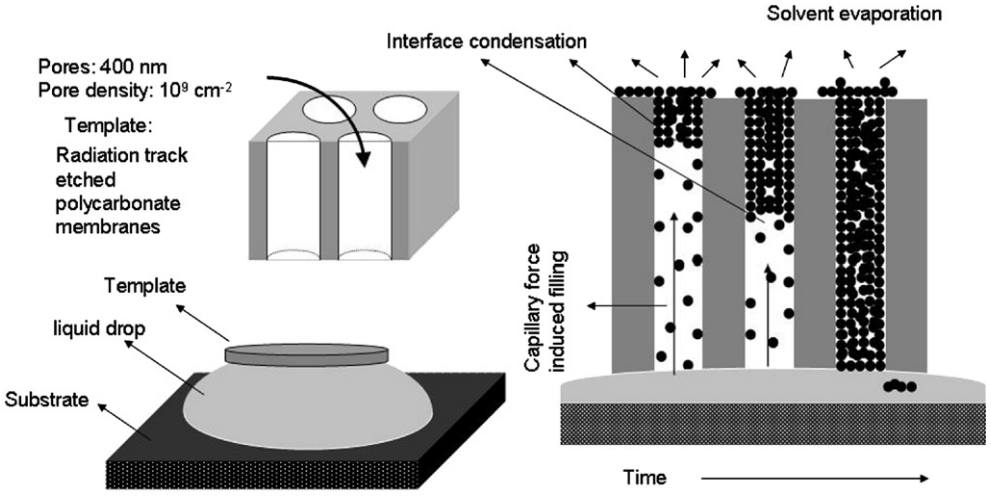

Fig. 19. Schematics of fabrication process of V_2O_5–TiO_2 nanorod arrays or V_2O_5 nanorod arrays. Top picture on the left: three-dimensional view of a polycarbonate membrane; bottom picture on the left: set-up for fabrication of nanorod arrays; schematic on the right: growth process of nanorod arrays. [K. Takahashi, Y. Wang, K.H. Lee, and G.Z. Cao, Appl. Phys. A82 (2006) 27].

otherwise, if electrical field is applied on multiple-phase sols, different sol particles have difference surface charges and phase segregation will occur so that homogeneous composition of the product can not be obtained. Centrifugation force has been used to grow nanorod arrays as well. However, for multiple-phase systems, size and shape of different sol particles may differ, thus phase segregation may occur which will prevent the formation of homogeneous nanocomposite nanorods as well.

Takahashi et al. [120] has developed a simple solvent evaporation approach for the formation of nanorod arrays of composites. Fig. 18 shows typical SEM images of (a) pure V_2O_5 nanorod arrays (b)V_2O_5–TiO_2 composite nanorods (molar ratio V/Ti=50/50) grown in 400 nm PC membranes and fired at 485 °C for 1 h in air. These nanorods project from the surface of ITO substrate like bristles of a brush and the V_2O_5–TiO_2 composite nanorods are less smooth than pure V_2O_5 nanorods. Fig. 19 presents schematics that illustrate the fabrication procedure of the nanorod arrays. The V_2O_5–TiO_2 nanorods were grown by solution filling into PC template pores with capillary force. The solution was drawn up into and filled up the pores of PC membrane; the vapor in the solution evaporated from the top surface of the PC template. As the solvent evaporated from the surface and the concentration enriched at the top of the pores, precipitation or gelation occurred first at the top of the pores and subsequently proceeded throughout the entire pores. Solvent evaporation induced deposition provides a simple and elegant method for preparing composite nanorod arrays. Its mechanism is similar to that of slip casting [70].

6. Converting from reactive templates

Nanorods or nanowires can also be synthesized using consumable templates, though the resultant nanowires and nanorods are in general not ordered to form aligned arrays. Nanowires of compounds can be prepared using a template-directed reaction. First nanowires or nanorods of one constituent element is prepared, and then reacted with chemicals containing other desired element to form final products. Gates et al. [121] converted single crystalline trigonal selenium nanowires into single crystalline nanowires of Ag_2Se by reacting Se nanowires with aqueous $AgNO_3$ solutions at room temperature. Nanorods can also be synthesized by reacting volatile metal halide or oxide species with carbon nanotubes to form solid carbide nanorods with diameters between 2 and 30 nm and lengths up to 20 μm [122]. ZnO nanowires were prepared by oxidizing metallic zinc nanowires [123]. Twinned Zn_2TiO_4 spinel nanowires were synthesized using ZnO nanowires as a template [124]. The synthesis involves three steps: (1) ZnO nanowires are synthesized first, (2) a layer of Ti is coated on the surface of ZnO nanowires through vapor deposition, and (3) annealing at elevated temperatures in air to form desired phase through solid state reaction. Hollow nanotubules of MoS_2 of ~30 μm long and 50 nm in external diameter with wall thickness of 10 nm were prepared by filling a solution mixture of molecular precursors, $(NH_4)_2MoS_4$ and $(NH_4)_2Mo_3S_{13}$, into the pores of alumina membrane templates. Then the template filled with the molecular precursors was heated to an elevated temperature and the molecular precursors thermally decomposed into MoS_2 [125].

Certain polymers and proteins were also used to direct the growth of nanowires of metals or semiconductors. For example, Braun et al. [126] reported a two-step procedure to use DNA as a template for the vectorial growth of a silver nanorods of 12 μm in length and 100 nm in diameter. DNA strands both surface-immobilized and in solution are used to template the growth and organization of CdS through spontaneous nucleation and growth on the surface of λ-DNA in $Cd(NO_3)_2$ aqueous solution and Na_2S dissolved in a mixture of water and ethanol [127]. CdS nanowires were prepared by a polymer-controlled growth [128]. For the synthesis of CdS nanowires, cadmium ions were well distributed in a polyacrylamide matrix, and then the Cd^{2+} containing polymer was treated with thiourea (NH_2CSNH_2) solvothermally in ethylenediamine at 170 °C, resulting in degradation of polyacrylamide. Single crystal CdS nanowires of 40 nm in diameter and up to 100 μm in length with a preferential [001] orientation were obtained. Although more work reports the synthesis of inorganic nanorods or nanotubes using polymers or proteins as templates, oxide nanowires can also be used as templates for the synthesis of polymer nanotubes. For example, manganese oxide nanowires have been used for the

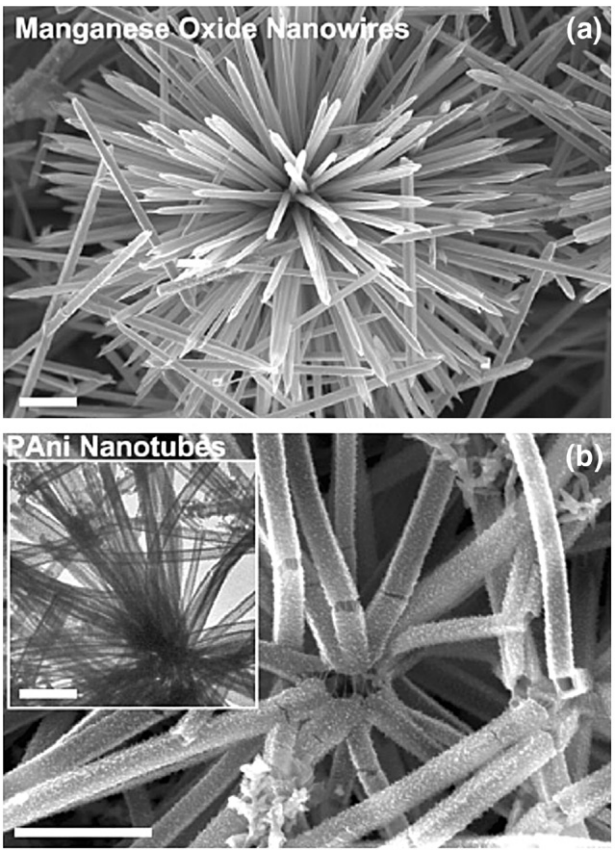

Fig. 20. Scanning electron microscopy (SEM) images of a) the cryptomelane-phase manganese oxide template and b) the resultant PAni nanotubes. The inset of (b) is the transmission electron microscopy (TEM) image of the PAni nanotubes. The scale bar is 1 μm. [L.J. Pan, L. Pu, Y. Shi, S.Y. Song, Z. Xu, R. Zhang, and Y.D. Zheng, Adv. Mater. 19 (2007) 461].

growth of polyaniline nanotubes [129]. During the synthesis, the manganese oxide nanowires are spontaneously removed by dissolving into acidic monomer solution through reduction reaction, while aniline monomer is oxidatively polymerized. Fig. 20 shows the SEM images of MnO_2 nanostructure templates and resultant polyaniline nanotubes.

Ordered nanotube arrays can be synthesized using reactive nanorod or nanotube arrays. For example, aligned carbon nanotubes have been used to grow TiO_2 nanotube arrays by electrophoretic deposition using TiO_2 sol as growth precursor [130]. Coaxial nanocable array is first formed with carbon nanotube as a core and TiO_2 as a shell. TiO_2 nanotube arrays are obtained when the carbon nanotubes are oxidization by heating the nanocable arrays at 600 °C in air for 2 h. Similarly, aligned carbon nanotubes can be used as templates for fabricating other nanocable or nanotube arrays. For example, coaxial conductive polymer–carbon nanotube arrays were synthesized through electrochemical deposition [131].

7. Summary and concluding remarks

This paper provides a brief summary of the fundamentals and technique approaches in template-based synthesis of nanowire or nanorod arrays. Examples are used to illustrate the growth of various nanorod materials with different technique approaches. The literature in this field is overwhelming and expands very rapidly. This chapter is by no means comprehensive in covering all the relevant literatures. Four groups of template-based synthesis methods have been reviewed and discussed in details. Electrochemical deposition or electrodeposition is the method for the growth of electrically conductive or semiconductive materials, such as metals, semiconductors, and conductive polymers and oxides. Electrophoretic deposition from colloidal dispersion is the method for the synthesis of dielectric nanorods and nanowires. Template filling is conceptually straightforward, though complete filling is often a great challenge. Converting of reactive templates is a method for both nanorod arrays and randomly oriented nanowires or nanorods, and often is combined with other synthetic methods.

This review has been focused on the growth of solid nanorod and nanowire arrays by template-based synthesis; however, template-based synthesis has been seen to attract an increasing attention for the synthesis of nanotubes, and in particular nanotube arrays [132]. One of the greatest advantages of template-based synthesis for the growth of nanotubes and nanotube arrays is the independent control of the length, diameter, and the wall thickness of the nanotubes. While the length and diameter of resultant nanotubes are dependent on the templates used for the synthesis, the wall thickness of nanotubes can be readily controlled by the growth duration. Another great advantage of template-based synthesis of nanotubes is the possibility of multilayered hollow nanotube or solid nanocable structures. For example, Ni–$V_2O_5{\cdot}nH_2O$ nanocable arrays have been synthesized by a two-step approach [133]. First Ni nanorod arrays were grown in PC template by electrochemical deposition and then the PC template was removed by pyrolysis, followed with sol electrophoretic deposition of $V_2O_5{\cdot}nH_2O$ on the surface of Ni nanorod arrays. It is obvious that there is a lot of space for more research activities in template-based synthesis of nanorod, nanotube and nanocable arrays and their applications [134].

This review is focused on the solution based growth of nanorod, nanowire and nanotube arrays. However, template-based synthesis has also been used for other synthesis methods. For example, atomic layer deposition (ALD) is a perfect technique for the synthesis or fabrication of alumina nanotube arrays with well controlled wall thickness and morphology [135]. ALD has also been employed for the fabrication of TiO_2 coated alumina membranes and TiO_2-coated Ni nanowires, and TiO_2 nanotube arrays were readily obtained by dissolving the templates [136].

Acknowledgements

This work has been supported in part by National Science Foundation (DMI-0455994 and DMR-0605159), Air Force Office of Scientific Research (AFOSR-MURI, FA9550-06-1-032). This work has also been supported by the Center for Nanotechnology at UW, Washington Technology Center, and Pacific Northwest National Laboratories (PNNL).

References

[1] Cao GZ. Nanostructures and nanomaterials: Synthesis, properties and applications. London: Imperial College Press; 2004.
[2] Nanowires and nanobelts: materials, properties and devices. In: Wang ZL, editor. Nanowires and Nonobelts of Functional Materials, vol. 2. Boston: Kluwer Academic Publishers; 2003.
[3] Xia YN, Yang P, Sun Y, Wu Y, Mayers B, Gates B, et al. Adv Mater 2003;15:353.
[4] Huczko A. Appl Phys A 2000;70:365.
[5] Burda C, Chen X, Narayanan R, El-Sayed MA. Chem Rev 2005;105:1025.
[6] Duan X, Lieber CM. Adv Mater 2000;12:298.
[7] Zach MP, Ng KH, Penner RM. Science 2000;290:2120.
[8] Wagner RS. In: Levitt AP, editor. Whisker Technology. New York: Wiley; 1970. p. 47.
[9] Givargizov EI. Highly Anisotropic Crystals. Dordrecht: Reidel; 1986.
[10] Kresge CT, Leonowicz ME, Roth WJ, Vartulli JC, Beck JS. Nature 1992;359:710.
[11] Corma A. Chem Rev 1997;97:2373.
[12] Singh N, Lyon LA. Chem Mater 2007;19:719.
[13] Furneaux RC, Rigby WR, Davidson AP. Nature 1989;337:147.
[14] Fleisher RL, Price PB, Walker RM. Nuclear Tracks in Solids. Berkeley: University of California Press; 1975.
[15] Tonucci RJ, Justus BL, Campillo AJ, Ford CE. Science 1992;258:783.
[16] Possin GE. Rev Sci Instrum 1970;41:772.
[17] Wu C, Bein T. Science 1994;264:1757.
[18] Fan S, Chapline MG, Franklin NR, Tombler TW, Cassell AM, Dai H. Science 1999;283:512.
[19] Enzel P, Zoller JJ, Bein T. Chem Commun 1992:633.
[20] Guerret-Piecourt C, Le Bouar Y, Loiseau A, Pascard H. Nature 1994;372:761.
[21] Ajayan PM, Stephan O, Redlich P, Colliex C. Nature 1995;375:564.
[22] Knez M, Bittner AM, Boes F, Wege C, Jeske H, Maiâ E, et al. Nano Lett 2003;3:1079.
[23] Gasparac R, Kohli P, Trofin MOML, Martin CR. Nano Lett 2004;4:513.
[24] Monson CF, Woolley AT. Nano Lett 2003;3:359.
[25] Weizmann Y, Patolsky F, Popov I, Willner I. Nano Lett 2004;4:787.
[26] Despic A, Parkhuitik VP. Modern Aspects of Electrochemistry, vol. 20. New York: Plenum; 1989.

[27] AlMawiawi D, Coombs N, Moskovits M. J Appl Phys 1991;70:4421.
[28] Foss CA, Tierney MJ, Martin CR. J Phys Chem 1992;96:9001.
[29] Mohler JB, Sedusky HJ. Electroplating for the Metallurgist, Engineer and Chemist. New York: Chemical Publishing; 1951.
[30] Bard AJ, Faulkner LR. Electrochemical Methods. New York: John Wiley & Sons; 1980.
[31] Nabarro FRN, Jackson PJ. In: Doremus RH, Roberts BW, Turnbull D, editors. Growth and Perfection of Crystals. New York: John Wiley; 1958.
[32] Whitney TM, Jiang JS, Searson PC, Chien CL. Science 1993;261:1316.
[33] Williams WD, Giordano N. Rev Sci Instrum 1984;55:410.
[34] Wang JG, Tian ML, Mallouk TE, Chan MHW. J Phys Chem B 2004;104:841.
[35] Wang HW, Russo B, Cao GZ. Nanotechnology 2006;17:2689.
[36] Jin CG, Jiang GW, Liu WF, Cai WL, Yao LZ, Yao Z, et al. J Mater Chem 2003;13:1743.
[37] Molares MET, Buschmann V, Dobrev D, Neumann R, Scholz R, Schuchert IU, et al. Adv Mater 2001;13:62.
[38] Yi G, Schwarzacher W. Appl Phys Lett 1999;74:1746.
[39] Brumlik CJ, Menon VP, Martin CR. J Mater Res 1994;268:1174.
[40] Brumlik CJ, Martin CR. J Am Chem Soc 1991;113:3174.
[41] Miller CJ, Widrig CA, Charych DH, Majda M. J Phys Chem 1988;92:1928.
[42] Tao FF, Guan MY, Jiang Y, Zhu JM, Xu Z, Xue ZL. Adv Mater 2006;18:2161.
[43] Han W, Fan S, Li Q, Hu Y. Science 1997;277:1287.
[44] Mallory G. In: Mallory GO, Hajdu JB, editors. Electroless plating: fundamentals and applications. Orlando, FL: AESF; 1990.
[45] Schönenberger C, van der Zande BMI, Fokkink LGJ, Henny M, Schmid C, Krüger M, et al. J Phys Chem B 1997;101:5497.
[46] Klein JD, Herrick II RD, Palmer D, Sailor MJ, Brumlik CJ, Martin CR. Chem Mater 1993;5:902.
[47] Hicks LD, Dresselhaus MS. Phys Rev B 1993;47:16631.
[48] Dresselhaus MS, Dresselhaus G, Sun X, Zhang Z, Cronin SB, Koga T. Phys Solid State 1999;41:679.
[49] Sander MS, Gronsky R, Sands T, Stacy AM. Chem Mater 2003;15:335.
[50] Lin C, Xiang X, Jia C, Liu W, Cai W, Yao L, Li X. J Phys Chem B 2004;108:1844.
[51] Xu DS, Xu YJ, Chen DP, Guo GL, Gui LL, Tang YQ. Adv Mater 2000;12:520.
[52] Lin C, Zhang G, Qian T, Li X, Yao Z. J Phys Chem B 2005;109:1430–2.
[53] Singh KV, Martinez-Morales AA, Andavan GTS, Bozhilov KN, Ozkan M. Chem Mater 2007;19:2446.
[54] Compton RG, Eklund JC, Marken F. J Electroanalysis 1997;9:509.
[55] Jérôme C, Jérôme R. Angew Chem Int Ed Engl 1998;37:2488.
[56] MacDiarmid AG. Rev Mod Phys 2001;73:701.
[57] Doblhofer K, Rajeshwar K. Handbook of Conducting Polymers. New York: Marcel Dekker; 1998. Chapter 20.
[58] Dauginet L, Duwez A-S, Legras R, Demoustier-Champagne S. Langmuir 2001;17:3952.
[59] Martin CR. Chem Mater 1996;8:1739.
[60] Martin CR. Adv Mater 1991;3:457.
[61] Hulteen JC, Martin CR. J Mater Chem 1997;7:1075.
[62] Liang L, Liu J, Windisch Jr CF, Exarhos GJ, Lin Y. Angew Chem Int Ed Engl 2002;41:3665.
[63] Takahashi K, Limmer SJ, Wang Y, Cao GZ. Jpn J Appl Phys B 2005;44:662.
[64] Hu CC, Chang KH, Lin MC, Wu YT. Nano Lett 2006;6:2690.
[65] Zheng MJ, Zhang LD, Li GH, Shen WZ. Chem Phys Lett 2002;363:123.
[66] Zhitomirsky I. Adv Colloid Interface Sci 2002;97:279.
[67] Van der Biest OO, Vandeperre LJ. Annu Rev Mater Sci 1999;29:327.
[68] Sarkar P, Nicholson PS. J Am Ceram Soc 1996;79:1987.
[69] Reed JS. Introduction to the principles of ceramic processing. New York: John Wiley & Sons; 1988.
[70] Hunter RJ. Zeta potential in colloid science: Principles and applications. London: Academic Press; 1981.
[71] Brinker CJ, Scherer GW. Sol–gel science: The physics and chemistry of sol–gel processing. San Diego: Academic Press; 1990.
[72] Pierre AC. Introduction to sol–gel processing. Norwell: Kluwer; 1998.
[73] Wright JD, Sommerdijk NAJM. Sol–gel materials: chemistry and applications. Amsterdam: Gordon and Breach; 2001.
[74] Everett DH. Basic principles of colloid science. London: the Royal Society of Chemistry; 1988.
[75] Callister WD. Materials science and engineering: an introduction. New York: John Wiley & Sons; 1997.
[76] Limmer SJ, Seraji S, Forbess MJ, Wu Y, Chou TP, Nguyen C, et al. Adv Mater 2001;13:1269.
[77] Limmer SJ, Seraji S, Forbess MJ, Wu Y, Chou TP, Nguyen C, et al. Adv Func Mater 2002;12:59.
[78] Limmer SJ, Cao GZ. Adv Mater 2003;15:427.
[79] Limmer SJ, Chou TP, Cao GZ. J Mater Sci 2004;39:895.
[80] Limmer SJ, Vince Cruz S, Cao GZ. Appl Phys A 2004;79:421.
[81] Limmer SJ, Chou TP, Cao GZ. J Sol–Gel Sci Technol 2005;36:183.
[82] Limmer SJ, Hubler TL, Cao GZ. J Sol–Gel Sci Technol 2003;26:577.
[83] Wang YC, Leu IC, Hon MN. J Mater Chem 2002;12:2439.
[84] Miao Z, Xu D, Ouyang J, Guo G, Zhao Z, Tang Y. Nano Lett 2002;2:717.
[85] Natarajan C, Nogami G. J Electrochem Soc 1996;143:1547.
[86] Lakshmi BB, Dorhout PK, Martin CR. Chem Mater 1997;9:857.
[87] Pan D, Shuyuan Z, Chen Y, Hou JG. J Mater Res 2002;17:1981.
[88] Petkov V, Trikalitis PN, Bozin ES, Billinge SJL, Vogt T, Kanatzidis MG. J Am Chem Soc 2002;124:10157.
[89] van der Drift A. Philips Res Rep 1968;22:267.
[90] Cao GZ, Schermer JJ, van Enckevort WJP, Elst WALM, Giling LJ. J Appl Phys 1996;79:1357.
[91] Ohring M. Materials science of thin films. San Diego: Academic Press; 2001.
[92] Takahashi K, Limmer SJ, Wang Y, Cao GZ. J Phys Chem B 2004;108:9795.
[93] Cao GZ. J Phys Chem B 2004;108:19921.
[94] Penn RL, Banfield JF. Geochim Cosmochim Acta 1999;63:1549.
[95] Chun CM, Navrotsky A, Aksay IA. Proc Microsc Microanal 1995:188.
[96] Livage J. Chem Rev 1998;178–180:999.
[97] Saban KV, Thomas J, Varughese PA, Varghese G. Cryst Res Technol 2002;37:1188.
[98] Grier D, Ben-Jacob E, Clarke R, Sander LM. Phys Rev Lett 1986;56:1264.
[99] Li CJ, Guo YG, Li BS, Wang CR, Wan LJ, Bai CL. Adv Mater 2005;17:71.
[100] Guo YG, Li CJ, Wan LJ, Chen DM, Wang CR, Bai CL, et al. Adv Func Mater 2003;13:626.
[101] Lakshmi BB, Patrissi CJ, Martin CR. Chem Mater 1997;9:2544.
[102] Lu Q, Gao F, Komarneni S, Mallouk TE. J Am Chem Soc 2004;126:8650.
[103] Polyakov B, Daly B, Prikulis J, Lisauskas V, Vengalis B, Morris MA, et al. Adv Mater 2006;18:1812.
[104] Huber CA, Huber TE, Sadoqi M, Lubin JA, Manalis S, Prater CB. Science 1994;263:800.
[105] Zhang Z, Gekhtman D, Dresselhaus MS, Ying JY. Chem Mater 1999;11:1659.
[106] Wolff EG, Coskren TD. J Am Ceram Soc 1965;48:279.
[107] Liang W, Martin CR. J Am Chem Soc 1990;112:9666.
[108] Marinakos SM, Brousseau III LC, Jones A, Feldheim DL. Chem Mater 1998;10:1214.
[109] Sun HD, Tang ZK, Chen J, Li G. Solid State Commun 1999;109:365.
[110] Cai Z, Lei J, Liang W, Menon V, Martin CR. Chem Mater 1991;3:960.
[111] Chen Y, Zhang LN, Lu XY, Zhao N, Xu J. Macromol Mater Eng 2006;291:1098.
[112] Tao SL, Desai TA. Nano Lett 2007;7:1463.
[113] Barrett C, Iacopino D, O'Carroll D, De Marzi G, Tanner DA, Quinn AJ, et al. Chem Mater 2007;19:338.
[114] Han YJ, Kim JM, Stucky GD. Chem Mater 2000;12:2068.
[115] Liu J, Fryxell GE, Qian M, Wang L-Q, Wang Y. Pure Appl Chem 2000;72:269.
[116] Chen L, Klar PJ, Heimbrodt W, Brieler F, Fröba M. Appl Phys Lett 2000;76:3531.
[117] Petkov N, Platschek B, Morris MA, Holmes JD, Bein T. Chem Mater 2007;19:1376.

[118] Limmer SJ, Hubler TL, Cao GZ. J Sol–Gel Sci Technol 2003;26:577.
[119] Wen T, Zhang J, Chou TP, Limmer SJ, Cao GZ. J Sol–Gel Sci Technol 2005;33:193.
[120] Takahashi K, Wang Y, Lee KH, Cao GZ. Appl Phys A 2006;82:27.
[121] Gates B, Wu Y, Yin Y, Yang P, Xia Y. J Am Chem Soc 2001;123:11500.
[122] Wong EW, Maynor BW, Burns LD, Lieber CM. Chem Mater 1996;8:2041.
[123] Li Y, Cheng GS, Zhang LD. J Mater Res 2000;15:2305.
[124] Yang Y, Sun W, Tay BK, Wang JX, Dong ZL, Fan HM. Adv Mater 2007;19:1839.
[125] Zelenski CM, Dorhout PK. J Am Chem Soc 1998;120:734.
[126] Braun E, Eichen Y, Sivan U, Ben-Yoseph G. Nature 1998;391:775.
[127] Dong LQ, Hollis T, Connolly BA, Wright NG, Horrocks BR, Houlton A. Adv Mater 2007;19:1748.
[128] Zhan J, Yang X, Wang D, Li S, Xie Y, Xia Y, et al. Adv Mater 2000;12:1348.
[129] Pan LJ, Pu L, Shi Y, Song SY, Xu Z, Zhang R, et al. Adv Mater 2007;19:461.
[130] Yang YD, Qu LT, Dai LM, Kang TS, Durstock M. Adv Mater 2007;19:1239.
[131] Gao M, Huang S, Dai L, Wallace G, Gao R, Wang Z. Angew Chem Int Ed Engl 2000;39:3664.
[132] Wang Y, Takahashi K, Shang HM, Cao GZ. J Phys Chem B 2005;109:3085.
[133] Takahashi K, Wang Y, Cao GZ. J Phys Chem B 2005;109:48.
[134] Wang Y, Takahashi K, Lee KH, Cao GZ. Adv Func Mater 2006;16:1133.
[135] Wang CC, Kei CC, Yu YW, Perng TP. Nano Lett 2007;7:1566.
[136] Kemell M, Pore V, Tupala J, Ritala M, Leskela M. Chem Mater 2007;19:1816.